https://doi.org/10.5194/acp-2019-785
Preprint. Discussion started: 11 September 2019

Atmospheric Chemistry and Physics Discussions

Vertical profiles of light absorption and scattering associated with black-carbon particle fractions in the springtime Arctic above 79°N

W. Richard Leaitch[1], John K. Kodros[2], Megan D. Willis[3, a], Sarah Hanna[4], Hannes Schulz[5], Elisabeth Andrews[6,8], Heiko Bozem[7], Julia Burkart[3, b], Peter Hoor[7], Felicia Kolonjari[1], John A. Ogren[8], Sangeeta Sharma[1], Meng Si[4], Knut von Salzen[9], Allan K. Bertram[4], Andreas Herber[5], Jonathan P. D. Abbatt[3], Jeffrey R. Pierce[2]

[1] - Environment and Climate Change Canada, Toronto, ON, Canada
[2] – Department of Atmospheric Science, Colorado State University, Fort Collins, CO, USA
[3] – Department of Chemistry, University of Toronto, Toronto, ON, Canada
[a] – now: Lawrence Berkeley National Laboratory, Chemical Sciences Division, Berkeley, CA, USA
[b] - now: Aerosol Physics and Environmental Physics, University of Vienna, Austria
[4] – Department of Chemistry, University of British Columbia, Vancouver, BC, Canada
[5] – Alfred Wegener Institute, Helmholtz Center for POLAR and Marine Research, Bremerhaven, Germany
[6] - University of Colorado, Boulder, CO, USA
[7] – Institute of Atmospheric Physics, Johannes Gutenberg-University, Mainz, Germany
[8] - National Oceanic and Atmospheric Administration (NOAA), Boulder, CO, USA
[9] - Environment and Climate Change Canada, Victoria, BC, Canada

Correspondence to: W. Richard Leaitch (leaitchs@gmail.com); Jeffrey R. Pierce (jeffrey.pierce@colostate.edu)

https://doi.org/10.5194/acp-2019-785
Preprint. Discussion started: 11 September 2019

Atmospheric Chemistry and Physics Discussions

Abstract. Despite the potential importance of black carbon (BC) to radiative forcing of the Arctic atmosphere, vertically-resolved measurements of the particle light scattering coefficient (σ_{sp}) and light absorption coefficient (σ_{ap}) in the springtime Arctic atmosphere are infrequent, especially measurements at latitudes at or above 80°N. Here, relationships among vertically-distributed aerosol optical properties (σ_{ap}, σ_{sp}, and single scattering albedo or SSA), particle microphysics and particle chemistry are examined for a region of the Canadian archipelago between 79.9°N and 83.4°N from near the surface to 500 hPa. Airborne data collected during April, 2015, are combined with ground-based observations from the observatory at Alert, Nunavut and simulations from the GEOS-Chem-TOMAS model (Kodros et al., 2018) to increase our knowledge of the effects of BC on light absorption in the Arctic troposphere. The results are constrained for σ_{sp} less than 15 Mm^{-1}, which represent 98% of the observed σ_{sp}, because the single scattering albedo (SSA) has a tendency to be lower at lower σ_{sp}, resulting in a larger relative contribution to Arctic warming. At 18.4 $m^2 g^{-1}$, the average BC mass absorption coefficient (MAC) from the combined airborne and Alert observations is substantially higher than the two averaged modelled MAC values (9.5 $m^2 g^{-1}$ and 7.0 $m^2 g^{-1}$) for two different internal mixing assumptions, the latter of which is based on previous observations. The higher observed MAC value may be explained by an underestimation of BC and possible differences in BC microphysics and morphologies between the observations and model. We present σ_{ap} and SSA based on the assumption that σ_{ap} is overestimated in the observations in addition to the assumption that the higher MAC is explained. Median values of the measured σ_{ap}, rBC and organic component of particles all increase by a factor of 1.8±0.1 going from near-surface to 750 hPa, and values higher than the surface persist to 600 hPa. Modelled BC, organics, and σ_{ap} agree with the near-surface measurements, but do not reproduce the higher values observed between 900 hPa and 600 hPa. The differences between modelled and observed optical properties follow the same trend as the differences between the modelled and observed concentrations of the carbonaceous components (black and organic). Some discrepancies in the model may be due to the use of a relatively low imaginary refractive index of BC as well as by the ejection of biomass burning particles only into the boundary layer at sources. For the assumption of the higher observed MAC value, the SSA range between 0.88 and 0.94, which is significantly lower than other recent estimates for the Arctic, in part reflecting the constraint of σ_{sp} <15 Mm^{-1}. The large uncertainties in measuring optical properties and BC as well as the large differences between measured and modelled values, here and in the literature, argue for improved measurements of BC and light absorption by BC as well as more vertical profiles of aerosol chemistry, microphysics, and other optical properties in the Arctic.

https://doi.org/10.5194/acp-2019-785
Preprint. Discussion started: 11 September 2019

Atmospheric Chemistry and Physics Discussions

1 Introduction

Aerosol particles responsible for Arctic haze (Mitchell, 1956) originate from mid-latitude pollution sources during winter and spring (e.g. Holmgren et al., 1974; Rahn et al., 1977; Rahn, 1981; Shaw, 1983; Barrie and Hoff, 1985; Radke et al., 1984; Schnell and Raatz, 1984; Barrie, 1986). During late spring and summer, the Arctic is cleansed of haze particles by increased levels of precipitation (e.g. Garrett et al., 2011) resulting in a much cleaner, sometimes pristine, troposphere. At lower altitudes, Europe and Northern Asia are thought to be the dominant source regions of Arctic haze with contributions from south/central Asian sources dominating at higher altitudes (e.g. Stohl, 2006; Fisher et al., 2011; Sharma et al., 2013; Qi et al., 2017; Xu et al., 2017). Although surface-based concentrations of Arctic haze components have declined since studies of Arctic haze first began (Heidam et al., 1999; Sirois and Barrie, 1999; Sharma et al., 2004; 2006; Quinn et al., 2009; Hirdman et al., 2010; Sinha et al., 2017), it is unclear how total atmospheric burdens have changed (e.g. Sharma et al., 2013).

Radiative forcing by Arctic haze particles may be an important regional driver of Arctic climate change (e.g. Law and Stohl, 2007; Quinn et al., 2008). Characterized by a unimodal number distribution centered between 200 and 300 nm diameter (e.g. Bigg, 1980; Heintzenberg, 1980; Radke et al., 1984; Leaitch et al., 1989; Staebler, 1994), the effectiveness of Arctic haze particles at scattering light (e.g. Delene and Ogren, 2002; Schmeisser et al., 2017) is one reason why the net effect of the Arctic aerosol has been estimated to cool the Arctic atmosphere (Najafi et al., 2015; Navarro et al., 2016). Black carbon (BC) is the primary anthropogenic light-absorbing component of Arctic haze, (e.g. Leighton, 1983; Valero et al., 1984; Blanchet and List, 1987; Valero et al., 1989; Pueschel and Kinne, 1995; Hansen and Nazarenko, 2004; Flanner et al., 2007; McConnell et al., 2007; Law and Stohl, 2007; Quinn et al., 2008; Schindell and Faluvegi, 2009; Brock et al., 2011). Mitigation of BC emissions has been proposed as a provisional means of slowing Arctic warming (Shindell and Faluvegi, 2008; Kopp and Mauzerall, 2010; Stohl et al., 2015; Sand et al., 2016), but considerable uncertainty surrounds radiative forcing by BC in the Arctic, in part due to the lack of observational data on the distribution of BC with altitude (e.g. Samset et al., 2013).

Here, we use a combination of airborne and ground-based observations plus modelling to examine particle light scattering coefficients (σ_{sp}), light absorption coefficients (σ_{ap}), and single scatter albedos (SSA) at the green wavelength of 550 nm from near the surface to 500 hPa over a region of the Arctic Ocean between 79.9°N and 83.4°N. Recent Arctic studies, ground-based and airborne, indicate SSA values ranging from 0.92 to

https://doi.org/10.5194/acp-2019-785
Preprint. Discussion started: 11 September 2019


Atmospheric Chemistry and Physics Discussions

0.97 during the month of April for a wavelength of 550 nm (Delene and Ogren, 2002; Brock et al., 2011; McNaughton et al., 2011; Schmeisser et al., 2017), or roughly 5% of the light incident on a population of Arctic haze particles is absorbed. This work, part of the Canadian Network on Climate and Aerosols: Addressing Key Uncertainties in Remote Canadian Environments or NETCARE, contributes knowledge concerning Arctic optical properties and warming of the Arctic lower troposphere by BC during April at higher latitudes.

Airborne measurements of σ_{ap} that are based on transmission of light through a filter, as used here, are constrained by instabilities during changes in pressure (i.e. altitude) and generally higher detection limits (DL) associated with flight conditions. To reduce the skewness of observations imposed by these constraints, we expand our dataset of σ_{ap} values by employing a linear relationship between measured σ_{ap} and the refractory black carbon mass concentrations (rBC) of Schulz et al. (2018). This approach enables a more comprehensive representation of values below DL. In the airborne component of this dataset, over 98% of one-minute averages of σ_{sp} exceeding detection limit (0.9 Mm^{-1}) are below 15 Mm^{-1}. By constraining the discussion to values of σ_{sp} less than 15 Mm^{-1}, we address the largest component of Arctic haze exclusive of the direct influence from strong plumes. Since most Arctic pollution in April is from long-range transport, the lower σ_{sp} suggests that these particles on average spent longer times in the Arctic atmosphere and thus are more indicative of the "chronic" Arctic haze discussed by Brock et al. (2011). Further, the SSA for particle populations that fall within this constraint have been found to decrease more sharply with decreasing σ_{sp} (e.g. Targino et al., 2005; Andrews et al., 2011), indicating that absorption per particle is on average greater at lower σ_{sp}. Details of the methods employed are described in Section 2. In Section 3, results are presented and vertical profiles of σ_{ap} and SSA are compared with simulated values. Section 4 is a broader discussion of the results, and conclusions are given in Section 5.

2 Methods

2.1 Observations overview

Ten research flights were conducted in the Arctic using the Alfred Wegener Institute (AWI) POLAR 6 aircraft beginning on April 5, 2015 and ending on April 21, 2015. The first and only flight from Longyearbyen, Svalbard, Norway is not discussed here as it dealt with some instrument and sampling issues. Subsequently, four flights were conducted from Alert, Nunavut, Canada during April 7-9 (two flights on April 8), two flights from Eureka, Nunavut, Canada (April 11 and 13) and three flights from Inuvik, Northwest Territories, Canada on April 20-21

https://doi.org/10.5194/acp-2019-785
Preprint. Discussion started: 11 September 2019

Atmospheric Chemistry and Physics Discussions

(two flights on April 20). Tracks of the flights out of Alert and Eureka can be found in Kodros et al. (2018), Schulz et al. (2018) and Willis et al. (2018). The flights out of Inuvik were conducted within a 300 km radius of Inuvik (68.4°N; 133.7°W). Sampling of submicron particles from the POLAR 6 during NETCARE is discussed by Leaitch et al. (2016), Schulz et al. (2018) and Willis et al. (2018). All airborne and model data presented here are referenced to a temperature of 20°C and pressure of 1013.25 hPa. The POLAR 6 data are restricted to between 2 minutes after takeoff and 2 minutes prior to landing to avoid local contamination.

Ground-based observations of σ_{sp}, σ_{ap}, rBC and particle microphysics are routinely conducted at the Dr. Neil Trivett Global Atmospheric Watch Observatory at Alert, Nunavut (82.5°N, 62.5°W). The site is approximately 7 km south-east of the main Alert station that is operated by the Canadian Department of National Defense. The impact of the camp on observations at the Alert Observatory (hereafter, referred to as Alert) has been found to be insignificant for particles larger than about 50 nm diameter (Leaitch et al., 2018), and the observations are filtered for air arriving from within a 45° arc centred on the station. The Alert optical properties data reported here are for particles less than 1 μm diameter.

2.2 Aerosol optical measurements

Particle light scattering coefficients (σ_{sp}) at wavelengths of 450 nm, 550 nm and 700 nm were measured with a TSI Model 3563 three-wavelength volume integrating nephelometer on the POLAR 6 and at Alert. To account for the absence of a forward scattering measurement where the collimated light beam is dumped (i.e., truncation of the total scattering between 0-7° and 170-180°), the correction described by Anderson and Ogren (1998) was applied. A span check of the nephelometer calibration is routinely performed at Alert using CO_2, and span checks of the nephelometer used on the POLAR 6 were conducted before and after the study.

Values of σ_{ap} at Alert are derived from a three-wavelength Particle Soot Absorption Photometer (PSAP), as discussed by Sharma et al. (2017). The σ_{ap} on the POLAR 6 were measured using a Continuous Light Absorption Photometer (CLAP), a three-wavelength filter-based instrument operating at 467 nm, 528 nm and 652 nm. Based on the PSAP design, the CLAP, designed and built by NOAA, samples consecutively on one of eight spots on one 47 mm filter, which improves functionality in situations where filter changes are more difficult, such as remote sites and aircraft (Ogren et al., 2017). For both the PSAP and CLAP, the σ_{ap} are derived from the change in light transmission through a spot on the filter accumulating particles relative to light transmission through a reference spot. Both the PSAP and CLAP data were corrected for multiple scattering

https://doi.org/10.5194/acp-2019-785
Preprint. Discussion started: 11 September 2019


Atmospheric Chemistry and Physics Discussions

arising from the filter medium and accumulating particles using an empirically based algorithm described by Bond et al. (1999) and Ogren (2010). To avoid artifacts associated with filter disturbances due to rapid pressure fluctuations, the POLAR 6 absorption data are limited to in-flight pressure variations, as recorded within the nephelometer, of less than 2 hPa over a two-minute period encompassing each one-minute sample.

The estimated detection limits (DL) for σ_{ap} and σ_{sp} on the POLAR 6 are 0.75 Mm^{-1} and 0.9 Mm^{-1}, respectively, at 550 nm wavelength and for one-minute averages. The DL are calculated from the maximum of two times the standard deviation of the raw measurement during in-flight zeroes, which are also constrained to pressure variations of 2 hPa or less. The σ_{sp} DL was adjusted for the truncation correction, and the σ_{ap} DL was adjusted for multiple scattering. Of approximately 2000 one-minute averaged data points, collected over nine flights, 220 absorption data points remain after scrutiny for DL and pressure variations. Uncertainties in the POLAR 6 σ_{ap} are considered in Section 3.3.

The DLs for σ_{ap} and σ_{sp} measured at Alert are 0.1 Mm^{-1} for and 0.4 Mm^{-1}, respectively, and represent DLs for the one-hour averages of Alert data used here. Based on Sherman et al. (2015) and Ogren et al. (2017), uncertainties in σ_{ap} at 1 Mm^{-1} and σ_{sp} at 10 Mm^{-1} are 60% and 24% respectively. After discriminating for local influences and removal of compromised data (e.g. zeroes), the Alert data set comprises 1505 one-hour averages, or approximately 70% of the February-April, 2015 time period. The months of February and March are included to broaden the comparison with the model results.

The σ_{ap} from the POLAR 6 and from Alert were adjusted to the nephelometer wavelengths assuming a $1/\lambda$ relationship, and the σ_{ap}, σ_{sp} and SSA for both platforms are reported for wavelengths of 450 nm (blue), 550 nm (green) and 700 nm (red). The SSA, given by $\sigma_{sp}/(\sigma_{sp}+\sigma_{ap})$, were calculated for the green values of σ_{sp} and σ_{ap}.

2.3 rBC and Physical Measurements

Size distributions for particles with diameters in the range of 85 - 1000 nm were measured on the POLAR 6 using an Ultra High Sensitivity Aerosol Spectrometer (UHSAS, Droplet Measurement Technology Inc); hereafter, all particle sizes are given as diameters. The UHSAS is a laser-based aerosol spectrometer. Checks of concentration and sizing were done with nearly monodisperse particles of ammonium sulphate. Details of the measurements used here are discussed by Schulz et al. (2018). The size distributions from the UHSAS are used to estimate submicron particle volume concentrations. Submicron particle volume concentrations at Alert are

https://doi.org/10.5194/acp-2019-785
Preprint. Discussion started: 11 September 2019


Atmospheric Chemistry and Physics Discussions

estimated from size distribution measurements with a TSI 3034 SMPS, previously discussed by Leaitch et al. (2013; 2018). As discussed by Willis et al. (2018), size distributions from the UHSAS were compared with those from the TSI 3034 SMPS at the Alert from four flights when the POLAR 6 flew between 60 m and 200 m above the ocean (sea ice) surface a few kilometres north of Alert. The volume concentrations calculated from the two measurements for the 85-500 nm size range compared within 20% for all flights.

Refractory black carbon (rBC) was measured on the POLAR 6 using two Droplet Measurement Technologies Inc. Single Particle Soot Photometers (SP2). The SP2 detects individual particles using an intra-cavity Nd:YAG laser operating at 1064 nm. Incandescence from components of particles absorbing at 1064 nm (i.e. BC) is detected by a pair of photomultiplier tubes, and the peak amplitude of the thermal radiation is proportional to the mass of refractory material (Moteki and Kondo, 2007; Slowik et al., 2007). The detection range of the SP2 used here is 0.40 fg rBC to 323 fg rBC, or approximately 75-700 nm for a rBC density of 1.8 g cm^{-3} (Bond and Bergstrom, 2006). Mass calibrations are based on Aquadag particles (Acheson Industries) and Fullerene soot that were size selected using a differential mobility analyser. The mobility diameters were converted to rBC mass concentrations following Gysel et al. (2011). Sensitivity to Aquadag was scaled to ambient rBC by a factor of 0.70 ± 0.05 (Laborde et al., 2012; Moteki and Kondo, 2010; Sharma et al., 2017; Schulz et al., 2018). The rBC measurements from both SP2 instruments agreed closely. Schulz et al. (2018) describe the dataset used here, and they estimate the uncertainty at ±15%. The rBC measurements conducted at Alert, also made using a SP2, are discussed by Sharma et al. (2017).

Non-refractory aerosol mass concentrations were measured aboard POLAR 6 with an Aerodyne High Resolution Time-of-Flight Aerosol Mass Spectrometer (ToF-AMS) (DeCarlo et al., 2006). These measurements are described in detail by Willis et al. (2018). Briefly, the ToF-AMS measured non-refractory aerosol between about 70 – 700 nm. Detection limits for sulfate and total organic aerosol were 0.01 μg/m3 and 0.08 μg/m3, respectively.

Coarse particles (>2 μm diameter) on the POLAR 6 were measured with a GRIMM Model 1.129 Optical Particle Counter. Model 1.129 measures particles larger than 0.25 μm, but only the coarse particle concentrations are used here. As shown by comparisons with a Particle Measuring Systems FSSP-300 probe operated under one wing of the POLAR 6, the coarse particles tend to be sampled less effectively than the submicron particles, but they are still an indicator of the presence of coarse particles, and, more importantly, the coarse particles entering the POLAR 6 sample manifold.

https://doi.org/10.5194/acp-2019-785
Preprint. Discussion started: 11 September 2019

Atmospheric Chemistry and Physics Discussions

2.4 Modelling

The observations of σ_{scat}, σ_{ap} and SSA are compared to version 10.01 of the GEOS-Chem chemical-transport model (geos-chem.com), driven by MERRA re-analysis meteorology fields. The February-April 2015 simulation was preceded by a 2-month spin-up. This version of GEOS-Chem uses a horizontal resolution of 4 degrees latitude by 5 degrees longitude (approximately 440 km x 72 km in the flight region near Alert and Eureka, and 440 km x 200 km near Inuvik) with 47 vertical layers. Relevant to the observations presented here, 24 vertical layers cover the pressure region from the surface to 500 hPa, 12 of which are from the surface to 850 hPa spaced equally by 15.5 hPa. Aerosol microphysics is simulated using TwO Moment Aerosol Sectional (TOMAS) microphysics scheme (Adams and Seinfeld, 2002) coupled with GEOS-Chem (known as "GEOS-Chem-TOMAS"), including tracers for sulfate, BC, organic aerosol, sea salt, dust, and aerosol water. More details are found in Adams and Seinfeld (2002), Lee et al. (2013), Lee and Adams (2012), and Kodros et al. (2018). Here, particle water is excluded from the calculations because the observed particles were relatively dry: during the flights, the outside air temperature was -15°C or less and the measured temperature of air entering the nephelometer, which was situated near the CLAP, ranged between +14°C or greater, indicating very low values of relative humidity at the point of measurement; also, no significant particle water was indicated in the ToF-AMS data. Aerosol optical properties are calculated using monthly averaged aerosol mass and number concentrations with refractive indices from the Global Aerosol Dataset (GADS). To calculate aerosol optical properties, we assume two of the BC mixing states discussed by Kodros et al. (2018): 1) "Allcore", in which BC is fully mixed with other chemical species in a core-shell morphology within each size section, where BC forms the core of the particle and hydrophilic aerosol species form a concentric shell around the BC core; 2) "Rshell", in which BC is mixed within a particle, again as a core surrounded by hydrophilic species, but the size-dependent fraction of BC–containing particles core sizes and hydrophilic coating thicknesses are constrained by the observed sizes and the modelled BC mass concentration as described by Kodros et al. (2018). The Allcore state is less realistic because every particle contains a BC core, whereas Arctic observations identify BC in roughly 10-20% of the particles (e.g. Sharma et al., 2017). As a result, the Allcore mixing assumption overestimates absorption (e.g. Alvarado et al., 2016). Rshell, which is based on observations, has a smaller fraction of coating material participating in absorption enhancement, resulting in lower absorption compared with Allcore; Rshell absorption is higher than that for the externally mixed assumption (Kodros et al., 2018). The Mie code of Bohren and Huffman (1983) for two concentric spheres is used to calculate σ_{scat}, σ_{ap} and SSA.

https://doi.org/10.5194/acp-2019-785
Preprint. Discussion started: 11 September 2019


Atmospheric Chemistry and Physics Discussions

Emissions are derived from the Emissions Database for Global Atmospheric Research (EDGAR) Hemispheric Transport of Air Pollution (HTAP) version 2.2 (Janssens-Maenhout et al., 2015). Following Xu et al. (2017), BC and organic carbon emissions from gas flaring derived from the Evaluating the Climate and Air Quality Impacts of short-lived Pollutants (ECLIPSE) emission inventory (Klimont et al., 2017) are included. Biomass burning emissions are from the Fire Inventory from NCAR (FINN) for the year 2015 (Wiedinmyer et al., 2011), but the particles are only injected into the boundary layer in this case. Dust emissions follow the DEAD scheme (Zender et al., 2003), and sea-salt aerosol emissions are based on Jaeglé et al. (2011). The model assumes a refractive index for BC of 1.75-0.45i in the mid visible (Hess et al., 1998). The imaginary part of the index for BC is lower than some estimates (e.g. 0.65i from Pluchino et al., 1980; Kim et al., 2015). See Kodros et al. (2018) for more details of the application of this version of the model to the Arctic as well as a detailed discussion of the role of mixing state on absorption by BC.

The data used here are from two vertical columns of the model: one column includes Axel Heiberg Island and the Arctic Ocean west of the island; the second is all Arctic Ocean to the west and slightly north of Alert. Hereafter, the two grids are referred to as "Axel" and "NW Alert". They are centred on 78°N, 95°W and 86°N, 75°W, respectively, as indicated by the stars in Fig. 1. The model grid that includes Alert is not used in order to avoid problems that might be associated with modelling of the significant terrain of Ellesmere Island.

3 Results

In Section 3.1, we identify the strongest influences of dust on the σ_{ap} observed from the POLAR 6. In section 3.2, we consider the mass absorption coefficients (MAC) for BC based on the observations (Alert and POLAR 6) and the model, including MAC at low BC mass concentrations. In Section 3.3, we present the profile data of rBC, median σ_{ap}, median SSA, σ_{sp} as well as sulphate and organic mass concentrations, and compare with like quantities from the GEOS-Chem-TOMAS model. The regression between σ_{ap} and rBC is used to increase the number of σ_{ap} and SSA values, from which the medians are derived, enabling the influence of values below DL and during pressure changes to be better represented.

3.1 Dust absorption

Figure 2 shows the blue (450 nm), green (550 nm) and red (700 nm) σ_{ap} plotted as a function of rBC for the nine POLAR 6 flights. A number of points in the rBC range of 0.15-0.3 μg m^{-3} lie well above their respective linear

https://doi.org/10.5194/acp-2019-785
Preprint. Discussion started: 11 September 2019


Atmospheric Chemistry and Physics Discussions

regression lines. Those points represent measurements from two of the flights conducted out of Inuvik in plumes above 3 km with trajectories that trace back over Northern China and Mongolia. In Fig. 3, the scattering Ångström exponents for green-red wavelengths are plotted versus the number concentrations of particles larger than 2 μm. The Inuvik points are identified separately from the Alert and Eureka points, and the coarse particle influence associated with the Inuvik points is evident. The pattern of the lower Ångström exponent points (<0.8) versus increasing number concentrations of coarse particles agrees with the results of Hallar et al. (2015) for Asian dust measured at a mountain top in Colorado and with our general knowledge of aerosol optical properties (e.g. Aryal et al., 2014; Clarke et al., 2007; Russell et al., 2010). We assume the Inuvik points with a scattering Ångström exponent of less than 0.8 and coarse particle number concentrations greater than 0.5 cm^{-3} are strongly influenced by dust; although there is some evidence of dust associated with all the Inuvik points.

The SSA from both the POLAR 6 and Alert are plotted against σ_{sp} at 550 nm, in Fig. 4. The POLAR 6 points are from the POLAR 6 CLAP and Nephelometer measurements, and the dust-influenced points associated with the Inuvik flights are highlighted. The Alert data cover the period February, 2015 to April 14, 2015, when the POLAR 6 left that region. Alert data from February and March of 2015 are included in part to provide a larger comparison base with the model and in part to demonstrate consistency of the POLAR 6 data with those from Alert, since the latter only reaches into the 0.75 $Mm^{-1}<\sigma_{ap}<1.6$ Mm^{-1} region during February. As in previous observations (e.g Targino et al., 2005; Andrews et al., 2011; Schmeisser et al., 2018), lower values of SSA are more frequent at these smaller σ_{spt}. Hereafter, we only consider data that fall into the region of green $\sigma_{sp}<15$ Mm^{-1}, which represent 98% of the above-DL POLAR 6 data collected over Alert and Eureka and 85% of the above-DL Alert data (February to April 14, inclusive). With these constraints, significant contributions to σ_{ap} from dust are removed. As next discussed, this improves the linear regression of σ_{ap} with rBC.

3.2 Mass Absorption

The regression of σ_{ap} with rBC for the combined POLAR 6 and Alert data (April 1-14), constrained as just discussed, has a slope of 18.4 m^2g^{-1} and intercept of +0.15 (Fig. 5). In Fig. 5, separate regressions through the Alert data and through the POLAR 6 data overlap at a confidence level of greater than 95%. The σ_{ap}-rBC slope represents the average MAC of rBC in the measured particles, but this value is about twice that typically found

https://doi.org/10.5194/acp-2019-785
Preprint. Discussion started: 11 September 2019


Atmospheric Chemistry and Physics Discussions

for Arctic measurements at the green wavelength (e.g. 9.5 $m^2 g^{-1}$, McNaughton et al., 2011; 8 $m^2 g^{-1}$, Sharma et al., 2017; 9.8 $m^2 g^{-1}$, Zanatta et al., 2018). In Fig. 6a and 6b, modelled σ_{ap}, which include a significant dust presence in many cases, are plotted against modelled BC for the NW Alert and Axel grid boxes, respectively. Modelled MAC values when dust is included are 11.7 and 11.1 $m^2 g^{-1}$ for Allcore and Rshell, respectively. Removal of points with modelled dust concentrations greater than 1.5 $\mu g\ m^{-3}$ (arbitrary value) leaves modelled MAC values in the Allcore case of 9.30 and 9.62 $m^2 g^{-1}$ for NW Alert and Axel grids, respectively, and 6.94 and 7.08 $m^2 g^{-1}$ for NW Alert and Axel, respectively, in the Rshell case. The modelled Allcore results are consistent with the previous Arctic MAC values reported above. The lower Rshell results are more consistent with the MAC value estimated for "freshly emitted" BC (e.g. 7.5 $m^2 g^{-1}$, Bond et al., 2006; Kahnert, 2010), due to a smaller influence of the coating material on absorption enhancement relative to the Allcore case.

The σ_{ap}-rBC regressions of the observations and the simulations both have positive intercepts. The intercepts are the result of increases in individual MAC values with decreasing concentrations of BC, as shown in Fig. 7a for the model and 7b for the observations; in these plots, MAC should be constant across all BC if absorption is solely due to BC without enhancements, such as lensing. In the case of the modelled MAC values, the persistence of dust concentrations at low BC concentrations (Fig. 7a) may have contributed to the increase in MAC at lower BC. As the BC concentrations decrease up to 100 times less than the dust concentrations, absorption by dust with its lower imaginary refractive index (0.0065 in the model) may approach absorption by BC, which would increase the apparent MAC for BC. Because the modelled organic aerosol (OA) concentrations decrease proportionately with decreasing BC (Fig. 7a) and the imaginary refractive index is lower (0.0055), absorbing OA cannot explain the increased MAC at lower BC. Also, the higher modelled MAC at lower BC may have a contribution from an increase in the coating enhancement factor as the BC core decreases in size.

In terms of the observations, absorbing dust may be present at lower BC concentrations, as shown in Fig. 7b. The mass concentrations of coarse particles, estimated from the POLAR 6 size distributions assuming a density of 2 $g\ cm^{-3}$, increase slightly with decreasing rBC concentrations. However, we cannot distinguish whether the composition of these coarse particles is dust or sea salt, and the 14 points with coarse particle mass concentrations of zero indicate only a stronger effect on MAC at decreasing BC (Fig. 7b). Thus, we rule out dust as a likely explanation for the higher MAC at lower BC in this case, leaving the following most viable explanations: (1) a greater deficiency in the rBC measurement at the lower BC concentrations, and (2) the presence of smaller BC fragments and/or more complex morphology of BC within the particles. According to Yu

https://doi.org/10.5194/acp-2019-785
Preprint. Discussion started: 11 September 2019


Atmospheric Chemistry and Physics Discussions

et al. (2019), the latter enhances absorption by factors of 3-16 within Arctic summer particles, when BC is also very low (Schulz et al., 2018).

The MAC-vs-BC curves in Fig. 7a and 7b have asymptotes in line with the MAC values determined from Fig. 5 and 6. Reasons for the higher observation-based MAC, based on the regression in Fig. 5, are unclear. There is no indication from the blue versus green slopes (Fig. 2) to suggest brown carbon is a significant factor for the Alert and Eureka data, and dust will not explain the differences in observed and modelled MAC. It is possible that a higher MAC is appropriate, as suggested by the recent observations in smoke plumes and in background particles over the continental U.S.A. (Mason et al., 2018), and by Yu et al (2019) as discussed above. Other possibilities to explain the higher observed MAC include the overestimation of absorption by the filter-based measurements, but as suggested by Lack et al. (2008) and Sinha et al. (2017) that is mostly related to absorption by organics and the up to 22% overestimation of absorption will not account for the present factor-of-two higher MAC value. Also, the σ_{ap} from the POLAR 6 and from Alert align well (Fig. 5). The present median σ_{ap} and SSA for Alert (0.50 Mm^{-1} and 0.95) are consistent with the April summary of Schmeisser et al. (2018: 0.45 Mm^{-1} and 0.95). The underestimation of BC is another potential factor in the higher MAC value. Sharma et al. (2017) found that filter-based thermo-optical measurements of elemental carbon were an average of 1.9 times higher than rBC measured at Alert, consistent with Bond et al. (2013), and which can explain the high MAC value of 18.4 m^2g^{-1}. In summary, two factors stand out as the most viable explanations for the higher MAC found here: underestimation of BC, and enhancement in absorption by BC due to the morphology of BC as a function of the size distribution.

As discussed in Section 3.3, the assumption of the higher BC MAC leads to substantially higher σ_{ap} and lower SSA aloft than indicated by either Brock et al. (2011) or McNaughton et al. (2011). Because we cannot resolve this issue, we add to our discussion the POLAR 6 plus Alert (Apr. 1-14) observations (Fig. 5) adjusted to MAC values of 9.2 $m^2\ g^{-1}$ and 7.0 $m^2\ g^{-1}$, through division of the σ_{ap} by factors of 2 and 2.62, respectively, as shown in Fig. 6c. The 9.2 $m^2\ g^{-1}$ is derived from an average of the three MAC values referenced above and the two modelled grids for the Allcore assumption, while the 7.0 $m^2\ g^{-1}$ is an average of the two modelled grids for the Rshell assumption. The results assuming the high MAC value is due to an overestimation of BC are shown in Fig. 6d. As in Fig. 6d, the high MAC value is referred to as rBC*2 and rBC*2.62 in Fig. 9 and 10 that show profiles of σ_{ap} and SSA, respectively, but that has no impact on the σ_{ap} and SSA derived from the high MAC.

https://doi.org/10.5194/acp-2019-785
Preprint. Discussion started: 11 September 2019

Atmospheric Chemistry and Physics Discussions

3.3 BC, Absorption, Scattering, SSA Vertical Distributions

We expand our dataset of σ_{ap} values by employing the linear regression between σ_{ap} and rBC shown in Fig. 5. This results in 956 σ_{ap} points instead of 220, but because the linear relationship does not fully account for variations of individual points, we restrict the profiles of σ_{ap} and SSA to median values calculated over approximately equal 50 hPa pressure intervals. Based on the linear fit, the uncertainty in the median σ_{ap} is 6% at a 99% confidence level, but that excludes possible biases in either the measurement of σ_{ap} or BC (as represented by rBC) discussed in Section 3.2. The corresponding uncertainty in the median SSA is ±0.01 or less for the range of SSA discussed here, again excluding possible biases.

Fig. 8 shows vertical profiles of the rBC measurements of Schulz et al. (2018) and the modelled BC. Modelled BC for April 1-14 and rBC overlap well for pressures >900 hPa. In the pressure region of 600-900 hPa, the modelled BC is about a factor of two lower than the POLAR 6 rBC: median rBC is 0.043 μg m^{-3}; median modelled BC for April 1-14 is 0.022 μg m^{-3}. Schulz et al. (2019) suggest the origin of the higher observed rBC between 600 hPa and 900 hPa is associated with emissions from gas flaring, industry and biomass burning over eastern Europe and western Russia. Willis et al. (2019) also pointed to biomass burning and gas flaring in Eurasia as possible sources of higher levels of carbonaceous particles, while noting that the lower altitude air masses had spent more than 10 days within the Polar Dome (defined for the present data by Bozem et al., 2019). Aerosol in the pressure range of about 800-650 hPa had entered the Polar Dome more recently, which may be consistent with the results of Xu et al. (2017) who used version 10.01 of GEOS-Chem (without TOMAS) and its adjoint to show that BC in this region was dominated by sources in eastern and southern Asia. The same version of GEOS-Chem is used here, with the notable exception that all biomass burning emissions were injected only within the boundary layer, potentially accounting for some of the low modelled BC relative to rBC.

Modelled profiles of σ_{ap} for April 1-14 and both the Axel and NW Alert grids are shown in Fig 9a for the Allcore assumption and in Fig. 9b for the Rshell assumption; major dust influence is removed, as shown as in Fig. 6a and 6b. Also shown in Fig. 9 are profiles of median values of the POLAR 6 rBC-based σ_{ap}, covering the period of April 7-13, inclusive, as well as the hourly σ_{ap} from Alert for April 1-14. The red POLAR 6 curve represents the assumption of absorption overestimation. The black POLAR 6 curve represents the higher MAC. The median σ_{ap} from the POLAR 6 agree reasonably with the corresponding Alert values. As expected, the modelled σ_{ap} based on the Allcore assumption are overall higher than those based on the Rshell assumption. The modelled values mostly fall in between the two sets of POLAR 6 σ_{ap} median values, except for pressures less than 600

https://doi.org/10.5194/acp-2019-785
Preprint. Discussion started: 11 September 2019


Atmospheric Chemistry and Physics Discussions

hPa, where the modelled values tend to be higher than either POLAR 6 curve. For pressures less than 600 hPa, the model and POLAR 6 both suggest an increasing tendency of σ_{ap} with decreasing pressure, consistent with Samset et al. (2013). At the surface, the modelled σ_{ap} overlap only with the Alert σ_{ap} based on the higher MAC.

Vertical profiles of SSA are shown in Fig. 10. The modelled results are for February, 2015, March, 2015, and April 1-14, 2015 with the upper (a-c) and lower panels (d-f) representing the Allcore and Rshell assumptions, respectively. Median values of the Alert SSA, calculated from the measured σ_{sp} and σ_{ap}, are shown for the corresponding model time period. The POLAR 6 SSA overlap well with the corresponding Alert SSA for April 1-14. The April 1-14 Alert SSA, based on the higher MAC, are the same as reported by Schmeisser et al. (2017) for Alert in April. The Alert SSA increase from February to April, which suggests a combination of the near-surface air cleansing itself of BC faster than the air in the lower troposphere during the high Arctic spring-to-summer transition and long-range transport aloft maintaining its influence longer than transport near the surface. Near the surface (>900 hPa), the modelled SSA are lower than the Alert and POLAR 6 results, in contrast to the modelled near-surface σ_{ap} that fall between the POLAR 6 and April 1-14 Alert results (Fig. 9). This difference is due to the modelled σ_{sp} being overall lower than the observed σ_{sp}, as discussed below in connection with Fig. 11. In Fig. 10, the modelled and observation-based SSA have opposite tendencies from the surface to about 600 hPa. In the 700-800 hPa region, there is good agreement between the modelled SSA for the Rshell mixing state and the observation-based SSA, but that agreement is inconsistent as the BC is underestimated (Fig. 8). The POLAR 6 near-surface (>950 hPa) and Alert SSA for early April range between 0.94 and 0.98, roughly consistent with the boundary layer SSA estimates of 0.97(+/-0.02) by Brock et al. (2011) and 0.95-0.96 by McNaughton et al. (2011). In the region of 600-900 hPa, the POLAR 6 SSA, for absorption overestimation, range between 0.94 and 0.96, which is also consistent with McNaughton et al. (2011) in this region and the "free tropospheric background haze" estimate of Brock et al. (2011). However, the SSA based on the higher MAC value range between 0.88 and 0.92 for the 600-900 hPa region, indicating substantially more absorption relative to scattering in this altitude range than found by Brock et al. (2011) and McNaughton et al. (2011). As above, a relatively low imaginary refractive index and ejection of biomass burning particles only into the boundary layer at the source are two factors that may contribute to the higher modelled SSA in the 600-900 hPa layer.

Modelled σ_{sp} for the April 1-14 period and observed σ_{sp} are shown in Fig. 11a; only the model results for the Axel grid are shown, as those for the NW Alert grid are similar. The modelled and observed σ_{sp} are most

https://doi.org/10.5194/acp-2019-785
Preprint. Discussion started: 11 September 2019


Atmospheric Chemistry and Physics Discussions

similar in the 600-900 hPa region, and therefore the differences between modelled and observation-based SSA (Fig. 10) in this pressure region are primarily the result of the variations in σ_{ap} (Fig. 9). Close to the surface (>900 hPa), the April 1-14 modelled σ_{sp} are lower than the POLAR 6 σ_{sp} and at the low end of the Alert σ_{sp}, which contributes to the lower modelled SSA relative to the observation-based SSA in Fig. 10. Near the surface, the modelled σ_{sp} for February agree best with the observed σ_{sp}, in part due to the higher submicron particle volumes simulated for February (Fig. 11b). The observed submicron volume concentrations are based on the UHSAS, and the modelled submicron volumes are calculated from the modelled mass concentrations of sulphate, organics and BC: (SO4/1.8 + Org/1.2 + BC/1.8), where 1.8, 1.2 and 1.8 are the respective densities of these components. The modelled scattering efficiency (scattering coefficient per unit volume) is significantly lower than the efficiency based on the observations. Near the surface (>900 hPa), the median of σ_{sp}/Volume from the observations is 12.1 μm^{-1} (range: 7.2-26.3) compared with 7.3 μm^{-1} (range: 5.6-10.3) from the model. For the pressure interval of 600-900 hPa, the median of σ_{scat}/Volume from the observations is 10.8 μm^{-1} (range: 6.2-36.4) versus 7.3 μm^{-1} (range: 5.6-12.2) from the model. Model underestimation of submicron particle sizes is a possible explanation for lower modelled volume scattering efficiencies. In addition, it is possible that the observed volumes, based on the UHSAS, are underestimated.

The vertical distribution of the median concentrations of organic mass (OM) and sulphate mass (from Willis et al., 2018) are shown in Fig. 12 along with modelled organic and sulphate mass concentrations for the Axel grid; results for the NW Alert grid are not appreciably different. The increase in rBC from the surface to about 650 hPa (Fig. 8) is paralleled by the increase in OM and its increase relative to sulphate. In Fig. 12, modelled OM near the surface (>900 hPa) is relatively close to the observed OM, but above that the observed OM is higher, by as much as a factor of two near 750 hPa. Near the surface, sulphate is underestimated by the model, which contributes to the model's lower volume and σ_{sp} (Fig. 11) and hence SSA near the surface (Fig. 10).

4. Discussion

Models tend to underestimate Arctic BC (Bond et al., 2013; Eckhardt et al., 2015) and sulphate (Eckhardt et al., 2015). Emissions are an important aspect of such comparisons, and a recent study using the ECHAM model showed that improved emissions inventories increase the annual BC burden over the Arctic by up to 30% (Schacht et al., 2019). The vertical distributions in Fig. 8 and 12 suggest that the BC emissions are coupled with

https://doi.org/10.5194/acp-2019-785
Preprint. Discussion started: 11 September 2019


Atmospheric Chemistry and Physics Discussions

other carbonaceous emissions producing OM. In this case, the tendency of rBC/OM is to increase with altitude, from approximately 5.8% near the surface to 7.3% at 650 hPa; 5.8% is equivalent to the slope of the modelled result in Fig. 7d. Variations in source emissions and secondary organic aerosol formation will explain some of the increase in rBC/OM throughout this altitude range, but precipitation scavenging preferentially removing more organic material than BC is also a possibility. In the high Arctic, the number fractions of particles larger than 100 nm that contain detectable rBC are <30% (e.g. Sharma et al., 2017; Kodros et al., 2018; references therein), which means there is significant potential for nucleation scavenging to separate OM (and sulphate) from BC as part of the precipitation process. As discussed by Targino et al. (2006) and Andrews et al. (2011), this may contribute to the general reduction in SSA at lower σ_{sp}.

The microphysics of the rBC components also supports the importance of wet deposition to the present observations. Schulz et al. (2019) showed that the mass mean diameter of the rBC components decreases with decreasing pressure from the surface, with an increase in the number of rBC-containing particles explaining the higher rBC mass concentrations aloft. Wet deposition by convective clouds near the source regions will lead to smaller BC components of particles aloft, if the larger-sized BC components are scavenged on average more than smaller BC components nearer the emissions sources. The stronger emissions from more distant and southerly regions reaching higher altitudes (Stohl, 2006; Xu et al., 2017) could explain the general increase in rBC number concentrations with altitude. An important role for particle microphysics, and in particular the representation of BC microphysics, in the modelling of BC transport to the Arctic is indicated. Despite the detailed microphysical model used here, the simulated BC vertical profiles suggest that the model transports more BC close to the surface. Excessive convective wet deposition that removes BC aloft (e.g. Mahmood et al., 2016) or re-distributes it to the near-surface region as well as the present modelled ejection of biomass burning particles only into the boundary layer are two potential reasons for the lower modelled BC in in this case. These results are consistent with Matsui et al. (2018), who point out that for models to properly simulate BC and its radiative impact on the Arctic atmosphere, they must have good representations of the microphysics and scavenging aspects of BC and other components of the aerosol. The results of Targino et al. (2005) and Andrews et al. (2011), suggesting lower SSA associated with lower σ_{sp}, as well as the present results are examples that wet scavenging may enhance the relative absorption by the Arctic aerosol, but at lower BC the possibility of significant contributions to absorption from small amounts of dust should be considered too.

https://doi.org/10.5194/acp-2019-785
Preprint. Discussion started: 11 September 2019


Atmospheric Chemistry and Physics Discussions

Many studies have shown that BC may be of great importance to Arctic warming (e.g. Bond et al., 2013), and models compare better with ground-based observations in the Arctic than aloft (e.g. Eckhardt et al., 2015, and present results). As discussed by Matsui et al. (2018) and indicated from the present work, representation of particle microphysics, including BC microphysics and scavenging of BC relative to all particles, is critical. There is a need for focussed airborne studies conducting high quality and comprehensive measurements of BC microphysics and optical properties in the Arctic, including better knowledge of the BC mass absorption coefficient across the particle size spectrum.

5. Conclusions

Relationships among vertically-distributed aerosol optical properties (σ_{abs}, σ_{scat}, and SSA), microphysics and particle chemistry were examined for a region of the Canadian archipelago between 79.9°N and 83.4°N from near the surface to 500 hPa. The airborne data were collected during April, 2015, and combined with ground-based observations from the observatory at Alert, Nunavut and simulations from the GEOS-Chem-TOMAS model (Kodros et al., 2018) in an effort to increase our knowledge of the effects of BC on absorption. The results were constrained for σ_{sp} less than 15 Mm^{-1}, which represents 98% of the observed σ_{sp}, or the longer-lived Arctic haze in this case.

Large uncertainties in estimating σ_{ap} and SSA are associated with this combined dataset. Based on observations from the POLAR 6 and Alert Observatory, the average mass absorption coefficient (MAC) for BC of 18.4 m^2g^{-1} was about twice the averaged modelled values of 9.2 m^2 g^{-1} and 7.0 m^2 g^{-1} (similar to some previous Arctic measurements) that represent different internal mixing assumptions discussed by Kodros et al. (2018). Although we cannot rule out overestimation of σ_{ap} in our observations, the higher MAC value is more likely a combination of the underestimation of BC and morphological arrangements of BC components within particles that are inconsistent with the often-used core-shell concept. Due to the uncertainties, we evaluated σ_{ap} and SSA assuming an overestimation of absorption in addition to the higher MAC value.

Measured σ_{abs}, rBC and organic material in the particles all increased by close to a factor of two going from the surface to 750 hPa. Modelled BC, organics, and σ_{ap} did not reflect the higher measured values in the 600-900 hPa region. The main sources of the differences between modelled and observed optical properties are the differences between the simulated and observed vertical distributions of rBC, organics and sulphate. As

https://doi.org/10.5194/acp-2019-785
Preprint. Discussion started: 11 September 2019


Atmospheric Chemistry and Physics Discussions

discussed, this highlights not only the importance of improving model emissions, deposition, and transport processes, but also microphysical details.

Assuming absorption overestimation, the SSA based on the POLAR 6 measurements ranged between 0.94 and 0.98, consistent with the results of Brock et al. (2011) and McNaughton et al. (2011). Assuming the measured MAC is explained by underestimation of BC and/or morphological features of BC components within particles, SSA ranged between 0.88 and 0.94, which is consistent with Schmeisser et al. (2017). The lower σ_{sp} (<15 Mm^{-1}) constraint has been shown to yield lower SSA values on average (Targino et al., 2005; Andrews et al., 2011; this work). The relatively high frequency of occurrence of σ_{sp} <15 Mm^{-1} in this region of the Arctic during April makes it important to understand the size distributions and morphology of BC in particles at these lower σ_{sp}. The present work suggests the need to consider low concentrations of dust at smaller BC concentrations as well as to be able to simulate size-distributed wet scavenging of BC.

This work typifies the large uncertainty that exists in our knowledge of the contribution from BC to direct warming of the Arctic atmosphere. It suggests a lower level of confidence in assessing direct absorption by BC, and the need for more detailed efforts if the impact of BC on Arctic climate is to be properly established. Those efforts include improved measurements of BC and absorption, and more vertical profiles of aerosol chemistry, microphysics and optical properties.

Acknowledgements

NETCARE was funded by the Natural Sciences and Engineering Research Council (NSERC) of Canada under its Climate Change and Atmospheric Research program, with additional financial and in-kind support from Environment and Climate Change Canada, Fisheries and Oceans Canada, the Alfred Wegener Institute, the Major Research Project Management Fund at the University of Toronto, and the Deutsche Forschungsgemeinschaft (DFG, German Research Foundation) – project number 268020496 – TRR 172, within the Transregional Collaborative Research Center "ArctiC Amplification: Climate Relevant Atmospheric and SurfaCe Processes, and Feedback Mechanisms (AC)3". Colorado State University researchers were supported by the US Department of Energy's Atmospheric System Research, an Office of Science, Office of Biological and Environmental Research program, under grant no. DE-SC0011780, the US National Science Foundation, Atmospheric Chemistry program, under grant no. AGS-1559607, and by the US National Oceanic and Atmospheric Administration, an Office of Science, Office of Atmospheric Chemistry, Carbon Cycle, and Climate

Program, under the cooperative agreement award no. NA17OAR430001. We gratefully acknowledge Kenn Borek Air Ltd, in particular our pilots and crew Garry Murtsell, Neil Traverse and Doug Mackenzie, for their support of our measurements. Logistical and technical support before and during the campaign was provided by a number of contributors, in particular by Desiree Toom (ECCC), Andrew Elford (ECCC), Dan Veber (ECCC), Julia Binder (AWI), Lukas Kandora (AWI), Jens Herrmann (AWI) and Manuel Sellmann (AWI). Extensive logistical and technical support was provided by Andrew Platt (ECCC), Mike Harwood (ECCC) and Martin Gerhmann (AWI). We are grateful to CFS Alert and Eureka Weather Station for supporting the measurements presented in this work.

References

- Adams, P. J. and Seinfeld, J. H.: Predicting global aerosol size distributions in general circulation models, J. Geophys. Res., 107, 4370, https://doi.org/10.1029/2001JD001010, 2002.
- Alvarado, M.J., Lonsdale, C.R., Macintyre, H.L., Bian, H., Chin, M., Ridley, D.A., Heald, C. L., Thornhill, K.L., Anderson, B.E., Cubison, M.J., Jimenez, J.L, Kondo, Y., Sahu, L.K., Dibb, J.E., and Wang, C.: Evaluating model parameterizations of submicron aerosol scattering and absorption with in situ data from ARCTAS 2008 Atmos. Chem. Phys., 16, 9435–9455, doi:10.5194/acp-16-9435-2016, 2016.
- Anderson, T. L. and Ogren, J. A.: Determining aerosol radiative properties using TSI 3563 integrating nephelometer, Aerosol Sci. Tech., 29, 57–69, 1998.
- Andrews, E., J.A. Ogren, P. Bonasoni, A. Marinoni, E. Cuevas, S. Rodriguez, J.Y. Sun, D. Jaffe, E. Fischer, U. Baltensperger, E. Weingartner, M. Collaud Coen, S. Sharma, A. Macdonald, W.R. Leaitch, N.-H. Lin, P. Laj, J. Stamenov, I. Kalapov, A. Jefferson, P. Sheridan, Climatology of Aerosol Radiative Properties in the Free Troposphere. Atmospheric Research, 102, 365-393, doi:10.1016/j.atmosres.2011.08.017, 2011.
- Aryal, R. P., Voss, K. J., Terman, P. A., Keene, W. C., Moody, J. L., Welton, E. J., and Holben, B. N.: Comparison of surface and column measurements of aerosol scattering properties over the western North Atlantic Ocean at Bermuda, Atmos. Chem. Phys.,
- 14, 7617–7629, doi:10.5194/acp-14-7617-2014, 2014.
- Barrie, L. A.: Arctic air pollution: An overview of current knowledge, Atmos. Environ., 20, 643–663, doi:10.1016/0004-6981(86)90180-0, 1986.
- Barrie, L. A. and Hoff, R. M.: Five years of air chemistry observations in the Canadian Arctic. Atmos. Environ., 19, 1995-2010, 1985.
- Bigg E. K.: Comparison of aerosol at four baseline monitoring stations. J. appl. Met. 19, 521-523, 1980.
- Blanchet J.-P. and R. List: Estimation of optical properties of Arctic Haze using a numerical model, Atmos.-Ocean, 21, 444 – 464, 1987.
- Bohren, C. F. and Huffman, D. R.: Absorption and scattering of light by small particles, Wiley Interscience, New York, USA, 1983.
- Bond, T. C., Anderson, T. L., and Campbell, D.: Calibration and intercomparison of filter-based measurements of visible light absorption by aerosols, Aerosol Sci. Tech., 30, 582–600, 1999.

https://doi.org/10.5194/acp-2019-785
Preprint. Discussion started: 11 September 2019

- Bond, T. C. and Bergstrom, R. W.: Light absorption by carbonaceous particles: an investigative review, Aerosol Sci. Tech., 40, 27–67, 2006.
- Bond, T. C., et al.: Bounding the role of black carbon in the climate system: A scientific assessment, J. Geophys. Res. Atmos., 118, 5380–5552, doi:10.1002/jgrd.50171, 2013.
- Brock, C. A., Cozic, J., Bahreini, R., Froyd, K. D., Middlebrook, A. M., McComiskey, A., Brioude, J., Cooper, O. R., Stohl, A., Aikin, K. C., de Gouw, J. A., Fahey, D. W., Ferrare, R. A., Gao, R.-S., Gore, W., Holloway, J. S., Hubler, G., Jefferson, A., Lack, D. A., Lance, S., Moore, R. H., Murphy, D. M., Nenes, A., Novelli, P. C., Nowak, J. B., Ogren, J. A., Peischl, J., Pierce, R. B., Pilewskie, P., Quinn, P. K., Ryerson, T. B., Schmidt, K. S., Schwarz, J. P., Sodemann, H., Spackman, J. R., Stark, H., Thomson, D. S., Thornberry, T., Veres, P., Watts, L. A., Warneke, C., and Wollny, A. G.: Characteristics, sources, and transport of aerosols measured in spring 2008 during the aerosol, radiation, and cloud processes affecting Arctic climate (ARCPAC) project, Atmos. Chem. Phys., 11, 2423–2453, doi:10.5194/acp-11-2423-2011, 2011.
- Clarke, A., McNaughton, C., Kapustin, V., Shinozuka, Y., Howell, S., Dibb, J., Zhou, J., Anderson, B., Brekhovskikh, V., Turner, H., and Pinkerton, M.: Biomass burning and pollution aerosol over North America: Organic components and their influence on spectral optical properties and humidification response, J. Geophys. Res., 112, D12S18, doi:10.1029/2006JD007777, 2007.
- Croft, B., Pierce, J.R., Martin, R.V., Hoose, C., Lohmann, U.: Uncertainty associated with convective wet removal of entrained aerosols in a global climate model, Atmospheric Chemistry and Physics, 12, 10725-10748, doi:10.5194/acp-12-10725-2012, 2012.
- Delene, D. and Ogren, J.A.: Variability of Aerosol Optical Properties at Four North American Surface Monitoring Sites. J. Atmos. Sci., 59, 1135-1150, 2002.
- Dymarska, M., Murray, B. J., Sun, L., Eastwood, M. L., Knopf, D. A., and Bertram, A. K.: Deposition ice nucleation on soot at temperatures relevant for the lower troposphere, J. Geophys. Res., 111, D04204, doi:10.1029/2005JD006627, 2006.
- Eckhardt, S., Quennehen, B., Olivié, D.J.L., Berntsen, T.K., Cherian, R., Christensen, J. H., Collins, W., Crepinsek, S., Daskalakis, N., Flanner, M., Herber, A., Heyes, C., Hodnebrog, Ø., Huang, L., Kanakidou, M., Klimont, Z., Langner, J., Law, K.S., Lund, M.T., Mahmood, R., Massling, A., Myriokefalitakis, S., Nielsen, I.E., Nøjgaard, J.K., Quaas, J., Quinn, P.K., Raut, J.-C., Rumbold, S.T., Schulz, M., Sharma, S., Skeie, R.B., Skov, H., Uttal, T., von Salzen, K., and Stohl, A.: Current model capabilities for simulating black carbon and sulfate concentrations in the Arctic atmosphere: a multi-model evaluation using a comprehensive measurement data set, Atmos. Chem. Phys., 15, 9413–9433, doi:10.5194/acp-15-9413-2015, 2015.
- Fisher, J. A., Jacob, D. J., Wang, Q., Bahreini, R., Carouge, C. C., Cubison, M. J., Dibb, J. E., Diehl, T., Jimenez, J. L., Leibensperger, E. M., Lu, Z., Meinders, M. B. J., Pye, H. O. T., Quinn, P. K., Sharma, S., Streets, D. G., van Donkelaar, A., and Yantosca, R. M.: Sources, distribution, and acidity of sulfate-ammonium aerosol in the Arctic in winter-spring, Atmos. Environ., 45, 7301-7318, doi:10.1016/j.atmosenv.2011.08.030, 2011.
- Flanner, M., Zender, C., Randerson, J. and Rasch, P.: Present-day climate forcing and response from black carbon in snow, J. Geophys. Res., 112, D11202, doi:10.1029/2006JD008003, 2007.
- Gysel, M., Laborde, M., Olfert, J. S., Subramanian, R., and Gröhn, A. J.: Effective density of Aquadag and fullerene soot black carbon reference materials used for SP2 calibration, Atmos. Meas. Tech., 4, 2851–2858, https://doi.org/10.5194/amt-4-2851-2011, 2011.
- Hallar, A.G., R. Petersen, E. Andrews, J. Michalsky, I. B. McCubbin, and J. A. Ogren: Contributions of dust and biomass burning to aerosols at a Colorado mountain-top site
- Atmos. Chem. Phys., 15, 13665–13679, doi:10.5194/acp-15-13665-2015, 2015.

- Hansen, J., and L. Nazarenko: Soot climate forcing via snow and ice albedos, Proc. Natl. Acad. Sci. U. S. A., 101, 423 – 428, doi:10.1073/pnas.2237157100, 2004.
- Heintzenberg J.: Particle size distribution and optical properties-of Arctic haze. Tellus 32, 251-260, 1980.
- Heidam, N. Z., Wåhlin, P., and Christensen, J.H.: Tropospheric gases and aerosols in northeast Greenland, J. Atmos. Sci., 56, 261-278, 1999.
- Hess, M., Koepke, P. and Schult, I.: Optical Properties of Aerosols and Clouds: The Software Package OPAC, Bulletin American Meteor. Soc., 79(5), 831–844, doi:https://doi.org/10.1175/1520-0477(1998)079<0831:OPOAAC>2.0.CO;2, 1998.
- Hirdman, D., Burkhart, J. F., Sodemann, H., Eckhardt, S., Jefferson, A., Quinn, P.K., Sharma, S., Ström, J., and Stohl, A.: Long-term trends of black carbon and sulphate aerosol in the Arctic: changes in atmospheric transport and source region emissions, Atmos. Chem. Phys., 10, 9351–9368, doi:10.5194/acp-10-9351-2010, 2010.
- Holmgren B., Shaw G. E. and Weller G.: Turbidity in the Arctic atmosphere, AIDJEX Bull., 27, 135-148, 1974.
- Jaeglé, L., Quinn, P. K., Bates, T. S., Alexander, B., and Lin, J.-T.: Global distribution of sea salt aerosols: new constraints from in situ and remote sensing observations, Atmos. Chem. Phys., 11, 3137–3157, https://doi.org/10.5194/acp-11-3137-2011, 2011.
- Janssens-Maenhout, G., Crippa, M., Guizzardi, D., Dentener, F., Muntean, M., Pouliot, G., Keating, T., Zhang, Q., Kurokawa, J., Wankmüller, R., Denier van der Gon, H., Kuenen, J. J. P., Klimont, Z., Frost, G., Darras, S., Koffi, B., and Li, M.: HTAP_v2.2: a mosaic of regional and global emission grid maps for 2008 and 2010 to study hemispheric transport of air pollution, Atmos. Chem. Phys., 15, 11411–11432, https://doi.org/10.5194/acp-15-11411-2015, 2015.
- Kahnert, M.: On the Discrepancy between Modeled and Measured Mass Absorption Cross Sections of Light Absorbing Carbon Aerosols, Aerosol Science and Technology, 44:6, 453-460, doi: 10.1080/02786821003733834, 2010.
- Kim, J., Bauer, H., Dobovičnik, T., Hitzenberger, R., Lottin, D., Ferry, D. and Petzold, A.: Assessing Optical Properties and Refractive Index of Combustion Aerosol Particles Through Combined Experimental and Modeling Studies, Aerosol Science and Technology, 49, 340-350, doi: 10.1080/02786826.2015.1020996, 2015.
- Klimont, Z., Kupiainen, K., Heyes, C., Purohit, P., Cofala, J., Rafaj, P., Borken-Kleefeld, J., and Schöpp, W.: Global anthropogenic emissions of particulate matter including black carbon, Atmos. Chem. Phys., 17, 8681–8723, https://doi.org/10.5194/acp-17-8681-2017, 2017.
- Kodros, J. K., Hanna, S., Bertram, A., Leaitch, W. R., Schulz, H., Herber, A., Zanatta, M., Burkart, J., Willis, M., Abbatt, J. 20 P. D. and Pierce, J. R.: Size-resolved mixing state of black carbon in the Canadian high Arctic and implications for simulated direct radiative effect, Atmospheric Chemistry and Physics Discussions, 1–32, doi:https://doi.org/10.5194/acp-2018-171, 2018.
- Kopp, R. E. and Mauzerall, D. L.: Assessing the climatic benefits of black carbon mitigation, P. Natl. Acad. Sci. USA, 107, 11703–11708, doi:10.1073/pnas.0909605107, 2010.
- Laborde, M., Mertes, P., Zieger, P., Dommen, J., Baltensperger, U., and Gysel, M.: Sensitivity of the Single Particle Soot Photometer to different black carbon types, Atmos. Meas. Tech., 5, 1031–1043, https://doi.org/10.5194/amt-5-1031-2012, 2012.

- Lack, D. A., C. D. Cappa, D. S. Covert, T. Baynard, P. Massoli, B. Sierau, T. S. Bates, P. K. Quinn, E. R. Lovejoy, and A. R. Ravishankara (2008), Bias in filter-based aerosol light absorption measurements due to organic aerosol loading: Evidence from ambient measurements, Aerosol Sci. Technol., 42(12), 1033–1041.
- Law, K. S. and Stohl, A.: Arctic air pollution: origins and impacts. Science, 315, 1537–1540, 2007.
- Leaitch, W.R., Hoff, R.M., and MacPherson, J.I.: Airborne and lidar measurements of aerosol and cloud particles in the troposphere over Alert Canada in April 1986. J. Atmos. Chem., 9, 187-211, 1989.
- Leaitch, W.R., S. Sharma, L. Huang, A. M. Macdonald, D. Toom-Sauntry, A. Chivulescu, K. von Salzen, J.R. Pierce, N.C. Shantz, A. Bertram, J. Schroder, A.-L. Norman, R.Y.-W. Chang: Dimethyl Sulphide Control of the Clean Summertime Arctic Aerosol and Cloud, Elementa: Science of the Anthropocene 1: 000017, doi: 10.12952/journal.elementa.000017, 2013.
- Leaitch, W. R., L. M. Russell, J. Liu, F. Kolonjari, D. Toom, L. Huang, S. Sharma, A. Chivulescu, D. Veber, and W. Zhang: Organic functional groups in the submicron aerosol at 82.5 N, 62.5W from 2012 to 2014, Atmos. Chem. Phys., 18, 1–19, doi.org/10.5194/acp-18-1-2018, 2018.
- Lee, Y. H. and Adams, P. J.: A Fast and Efficient Version of the TwO-Moment Aerosol Sectional (TOMAS) Global Aerosol Microphysics Model, Aerosol Sci. Technol., 46, 678–689, https://doi.org/10.1080/02786826.2011.643259, 2012.
- Lee, Y. H., Pierce, J. R., and Adams, P. J.: Representation of nucleation mode microphysics in a global aerosol model with sectional microphysics, Geosci. Model Dev., 6, 1221–1232, https://doi.org/10.5194/gmd-6-1221-2013, 2013.
- Leighton, H.: Influence of the Arctic Haze on the solar radiation budget. Atmos. Environ., 17, 2065-2068, 1983.
- Mahmood, R., Salzen, K., Flanner, M., Sand, M., Langner, J.,Wang, H., and Huang, L.: Seasonality of global and Arctic black carbon processes in the Arctic Monitoring and Assessment Programme models, J. Geophys. Res.-Atmos., 121, 7100–7116, 2016.
- Mason, B., Wagner, N.L., Adler, G., Andrews, E., Brock, C.A., Gordon, T.D., Lack, D.A., Perring, A.E., Richardson, M.S., Schwarz, J.P., Shook, M.A., Thornhill, K.L., Ziembad, L.D., and Murphy, D.M.: An intercomparison of aerosol absorption measurements conducted during the SEAC4RS campaign, Aerosol Sci. & Technol., 52, 1012–1027, doi.org/10.1080/02786826.2018.1500012, 2018.
- Matsui, H., Hamilton, D.S., and Mahowald, N.M.: Black carbon radiative effects highly sensitive to emitted particle size when resolving mixing-state diversity, Nat. Commun., doi: 10.1038/s41467-018-05635-1, 2018.
- McNaughton, C. S., A. D. Clarke, S. Freitag, V. N. Kapustin, Y. Kondo, N. Moteki, L. Sahu, N. Takegawa, J. P. Schwarz, J. R. Spackman, L. Watts, G. Diskin, J. Podolske, J. S. Holloway, A. Wisthaler, T. Mikoviny, J. de Gouw, C. Warneke, J. Jimenez, M. Cubison, S. G. Howell, A. Middlebrook, R. Bahreini, B. E. Anderson, E. Winstead, K. L. Thornhill, D. Lack, J. Cozic, and C. A. Brock (2011), Absorbing aerosol in the troposphere of the Western Arctic during the 2008 ARCTAS/ARCPAC airborne field campaigns, Atmospheric Chemistry and Physics, 11(15), 7561–7582, doi: 10.5194/acp-11-7561-2011.
- McConnell, J. R., Edwards, E., Kok, G. L., Flanner, M. G., Zender, C. S., Saltzman, E. S., Banta, J. R., Pasteris, D. R., Carter, M. M., and Kahl, J. D.: 20th-century industrial black carbon emissions altered Arctic climate, Science, 317, 1381–1384, 2007.
- Mitchell M.: Visual range in the polar regions with particular reference to the Alaskan Arctic. J. Atmos. Terr. Phys., Special Supplement, 195-211, 1956.Moteki, N. and Kondo, Y.: Effects of mixing state on black carbon

measurements by laser-induced incandescence, Aerosol Sci. Technol., 41, 398–417, https://doi.org/10.1080/02786820701199728, 2007.

- Moteki, N. and Kondo, Y.: Dependence of laser-induced incandescence on physical properties of black carbon aerosols: measurements and theoretical interpretation, Aerosol Sci. Tech., 44, 663–675, https://doi.org/10.1080/02786826.2010.484450, 2010.
- Najafi, M. R., Zwiers, F. W. and Gillett, N. P.: Attribution of Arctic temperature change to greenhouse-gas and aerosol 25 influences, Nature Clim. Change, 5(3), 246–249, doi:10.1038/nclimate2524, 2015.
- Navarro, J. C. A., Varma, V., Riipinen, I., Seland, Ø., Kirkevåg, A., Struthers, H., Iversen, T., Hansson, H.-C. and Ekman, A. M. L.: Amplification of Arctic warming by past air pollution reductions in Europe, Nature Geoscience, 9(4), 277–281, 30 doi:10.1038/ngeo2673, 2016.
- Ogren, J. A.: Comment on "Calibration and intercomparison of filter-based measurements of visible light absorption by aerosols", Aerosol Sci. Tech., 44, 589–591, 1608, doi.org/10.1080/02786826.2010.482111, 2010.
- Ogren, J.A., Wendell, J., Andrews, E., et al.:"Continuous Light Absorption Photometer for Long-Term Studies," Atmos Meas. Tech.,10, 4805-4818, doi:10.5194/amt-10-4805-2017, 2017.Pluchino A. B., Goldberg S. S., Dowling J. M. and Randall C. M: Refractive index measurements of single micron-sized carbon particles. Appl. Opt. 19, 3370-3372, 1980.
- Pueschel, R.F. and S.A. Kinne: Physical and radiative properties of Arctic atmospheric aerosols, Sci. Tot. Environ., 161, 811-824, 1995.
- Qi, L., Q. Li, D. K. Henze, H.-L. Tseng, and C. He: Sources of springtime surface black carbon in the Arctic: an adjoint analysis for April 2008, Atmos. Chem. Phys., 17, 9697–9716, doi:10.5194/acp-17-9697-2017, 2017.
- Quinn, P. K. and Coauthors, 2008: Short-lived pollutants in the Arctic: their climate impact and possible mitigation strategies. Atmos. Chem. Phys., 8(6), doi:10.5194/acp-8-1723-2008.
- Quinn, P.K., T. S. Bates, K. Schulz, and G. E. Shaw: Decadal trends in aerosol chemical composition at Barrow, Alaska: 1976–2008, Atmos. Chem. Phys., 9, 8883–8888, 2009.
- Radke L. F., Lyons J. H., Hegg D. A., Hobbs P. V. and Bailey I. H.: Airborne observations of Arctic aerosols-I. Characteristics of Arctic haze, Geophys. Res. Lett. 11, 393-396, 1984.
- Rahn K. A., Boyrs R. and Shaw G. E.: The Asian source of Arctic haze bands, Nature, 268, 713-715, 1977.
- Rahn K. A.: The Arctic air-sampling network in 1980, Atmos. Environ., 15, 1349-1352, 1981.
- Russell, P. B., Bergstrom, R. W., Shinozuka, Y., Clarke, A. D., De-Carlo, P. F., Jimenez, J. L., Livingston, J. M., Redemann, J., Dubovik, O., and Strawa, A.: Absorption Angstrom Exponent in AERONET and related data as an indicator of aerosol composition, Atmos. Chem. Phys., 10, 1155–1169, doi:10.5194/acp-10-1155-2010, 2010.
- Samset, B. H., Myhre, G., Schulz, M., Balkanski, Y., Bauer, S., Berntsen, T. K., Bian, H., Bellouin, N., Diehl, T., Easter, R. C., Ghan, S. J., Iversen, T., Kinne, S., Kirkevåg, A., Lamarque, J.-F., Lin, G., Liu, X., Penner, J. E., Seland, Ø., Skeie, R. B., Stier, P., Takemura, T., Tsigaridis, K., and Zhang, K.: Black carbon vertical profiles strongly affect its radiative forcing uncertainty, Atmos. Chem. Phys., 13, 2423-2434, https://doi.org/10.5194/acp-13-2423-2013, 2013.
- Sand, M., Berntsen, T. K., von Salzen, K., Flanner, M. G., Langner, J., and Victor, D. G: Response of the Arctic temperature to changes in emissions of short-lived climate forcers, Nat. Clim. Chang., 6, 286–289, https://doi.org/10.1038/nclimate2880, 2016.

https://doi.org/10.5194/acp-2019-785
Preprint. Discussion started: 11 September 2019

- Schacht, J., Heinold, B., Quaas, J., Backman, J., Cherian, R., Ehrlich, A., Herber, A., Huang, W. T. K., Kondo, Y., Massling, A., Sinha, P. R., Weinzierl, B., Zanatta, M., and Tegen, I.: The importance of the representation of air pollution emissions for the modeled distribution and radiative effects of black carbon in the Arctic, Atmos. Chem. Phys. Discuss., https://doi.org/10.5194/acp-2019-71, in review, 2019.
- Schmeisser, L., Backman, J., Ogren, J. A., Andrews, E., Asmi, E., Starkweather, S., Uttal, T., Fiebig, M., Sharma, S., Eleftheriadis, K., Vratolis, S., Bergin, M., Tunved, P., and Jefferson, A.: Seasonality of aerosol optical properties in the Arctic, Atmos. Chem. Phys. 18, 11599-11622, doi:10.5194/acp-18-11599-2018, 2018.
- Schnell R. C. and Raatz W. E.: Vertical and horizontal characteristics of Arctic hare during AGASP; Alaskan Arctic, Geophys. Res. Lett. 11, 369-376, 1984.
- Schulz, H., Bozem, H., Zanatta, M., Leaitch, W. R., Herber, A. B., Burkart, J., Willis, M. D., Hoor, P. M., Abbatt, J. P. D. and Gerdes, R.: High–Arctic aircraft measurements characterising black carbon vertical variability in spring and summer, 35 Atmospheric Chemistry and Physics Discussions, 1–34, doi:10.5194/acp-2018-587, 2018.
- Sirois, A., and L. A. Barrie: Arctic lower tropospheric aerosol trends and composition at Alert, Canada: 1980–1995, J. Geophys. Res., 104, 11,599–11,618, doi:10.1029/1999JD900077, 1999.
- Sharma, S., D. Lavoue, H. Cachier, L. A. Barrie, and S. L. Gong: Long-term trends of the black carbon concentrations in the Canadian Arctic, J. Geophys. Res., 109, D15203, doi:10.1029/2003JD004331, 2004.
- Sharma, S., E. Andrews, L. A. Barrie, J. A. Ogren, and D. Lavoue´: Variations and sources of the equivalent black carbon in the high Arctic revealed by long-term observations at Alert and Barrow: 1989–2003, J. Geophys. Res., 111, D14208, doi:10.1029/2005JD006581, 2006.
- Sharma, S., M. Ishizawa, D. Chan, D. Lavoue´, E. Andrews, K. Eleftheriadis, and S. Maksyutov: 16-Year Simulation of Arctic Black Carbon: Transport, Source Contribution, and Sensitivity Analysis on Deposition, J. Geophys. Res., 118, doi:10.1029/2012JD017774, 2013.
- Sharma, S., W. R. Leaitch, L. Huang, D. Veber, F. Kolonjari, W. Zhang, S. J. Hanna, A. K. Bertram, and J. A. Ogren: An evaluation of three methods for measuring black carbon in Alert, Canada, Atmos. Chem. Phys., 17, 15225–15243, doi.org/10.5194/acp-17-15225-2017, 2017.
- Shaw, G. E.: Evidence for a central Eurasian source area of Arctic haze in Alaska, Nature, 299, 815–818, 1983.
- Sherman, J. P., Sheridan, P. J., Ogren, J. A., Andrews, E., Hageman, D., Schmeisser, L., Jefferson, A., and Sharma, S.: A multi-year study of lower tropospheric aerosol variability and systematic relationships from four North American regions, Atmos. Chem. Phys., 15, 12487–12517, https://doi.org/10.5194/acp-15-12487-2015, 2015.
- Shindell, D. and G. Faluvegi: Climate response to regional radiative forcing in the twentieth century. Nature Geosci., 2(4), 294-300, doi: 10.1038/NGEO473, 2009.
- Sinha, P. R., Kondo, Y., Koike, M., Ogren, J. A., Jefferson, A., Barrett, T. E., Sheesley, R. J., Ohata, S., Moteki, N., Coe, H., Liu, D., Irwin, M., Tunved, P., Quinn, P. K., and Zhao, Y.: Evaluation of ground-based black carbon measurements by filter-based photometers at two Arctic sites, J. Geophys. Res. Atmos., 122, 3544–3572, doi:10.1002/2016JD025843, 2017.
- Slowik, J. G., Cross, E. S., Han, J.-H., Davidovits, P., Onasch, T. B., Jayne, J. T., Williams, L. R., Canagaratna, M. R., Worsnop, D. R., Chakrabarty, R. K., Moosmüller, H., Arnott, W. P., Schwarz, J. P., Gao, R.-S., Fahey, D. W.,

Kok, G. L., and Petzold, A.: An Inter-Comparison of Instruments Measuring Black Carbon Content of Soot Particles, Aerosol Sci. Technol., 41, 295–314, https://doi.org/10.1080/02786820701197078, 2007.

- Sinha, P. R., Y. Kondo, M. Koike, J. A. Ogren, A. Jefferson, T. E. Barrett, R. J. Sheesley, S. Ohata, N. Moteki, H. Coe, D. Liu , M. Irwin, P. Tunved, P. K. Quinn, and Y. Zhao: Evaluation of ground-based black carbon measurements by filter-based photometers at two Arctic sites, J. Geophys. Res. Atmos., 122, 3544–3572, doi:10.1002/2016JD025843, 2017.
- Sobhani, N., Kulkarni, S., and Carmichael, G.R.: Source sector and region contributions to black carbon and PM2:5 in the Arctic, Atmos. Chem. Phys., 18, 18123–18148, doi.org/10.5194/acp-18-18123-2018, 2018.
- Staebler, R.M., G. den Hartog, B. Georgi, and Thorsten Düsterdiek: Aerosol size distributions in Arctic haze during the POLAR Sunrise Experiment 1992, J. Geophys. Res., 99, 25,429-25,437, 1994.
- Stohl, A., Aamaas, B., Amann, M., Baker, L. H., Bellouin, N., Berntsen, T. K., Boucher, O., Cherian, R., Collins, W., Daskalakis, N., Dusinska, M., Eckhardt, S., Fuglestvedt, J. S., Harju, M., Heyes, C., Hodnebrog, Ø., Hao, J., Im, U., Kanakidou, M., Klimont, Z., Kupiainen, K., Law, K. S., Lund, M. T., Maas, R., MacIntosh, C. R., Myhre, G., Myriokefalitakis, S., Olivié, D., Quaas, J., Quennehen, B., Raut, J.-C., Rumbold, S. T., Samset, B. H., Schulz, M., Seland, Ø., Shine, K. P., Skeie, R. B., Wang, S., Yttri, K. E., and Zhu, T.: Evaluating the climate and air quality impacts of short-lived pollutants, Atmos. Chem. Phys., 15, 10529-10566, https://doi.org/10.5194/acp-15-10529-2015, 2015.
- Targino, A.C., Noone, K.J., Ostrom, E: Airborne in-situ characterization of dry aerosol optical properties in a multisource influenced marine region, Tellus 57B, 247–260, 2005.
- Valero F. P. J., Ackerman T. P. and Gore J. Y.: The absorption of solar radiation by the Arctic atmosphere during the haze season and its effects on the radiation balance. Geophys. Res. Lett. 11, 465-468, 1984.
- Valero, F.P.J., T.P. Ackerman, and W.J.R. Gore: The effects of the arctic haze as determined from airborne radiometric measurements during AGASP II, J. Atmos. Chem., 9, 225-244, 1989.
- Wiedinmyer, C., Akagi, S. K., Yokelson, R. J., Emmons, L. K., Al-Saadi, J. A., Orlando, J. J., and Soja, A. J.: The Fire Inventory from NCAR (FINN): a high resolution global model to estimate the emissions from open burning, Geosci. Model Dev., 4, 625–641, https://doi.org/10.5194/gmd-4-625-2011, 2011.
- Willis, M.D., Bozem, H., Kunkel, D., Lee, A.K.Y., Schulz, H., Burkart, J., Aliabadi, A.A., Herber, A.B., Leaitch, W.R., and Abbatt, J.P.D.: Composition and Sources of Springtime High Arctic Aerosol, Composition and Sources of Springtime High Arctic Aerosol, ACPD-2018-628, 2018.
- Xu, J.-W., Martin, R. V., Morrow, A., Sharma, S., Huang, L., Leaitch, W. R., Burkart, J., Schulz, H., Zanatta, M., Willis, M. D., Henze, D. K., Lee, C. J., Herber, A. B. and Abbatt, J. P. D.: Source attribution of Arctic black carbon constrained by aircraft and surface measurements, Atmospheric Chemistry and Physics, 17, 11971–11989, doi:10.5194/acp-17-11971-2017, 2017.
- Zanatta, M., Paolo Laj, Martin Gysel, Urs Baltensperger, Stergios Vratolis, Konstantinos Eleftheriadis, Yutaka Kondo, Philippe Dubuisson, Victor Winiarek, Stelios Kazadzis, Peter Tunved and Hand-Werner Jacobi: Effects of mixing state on optical and radiative properties of black carbon in the European Arctic, Atmos. Chem. Phys. Discuss., https://doi.org/10.5194/acp-2018-455, 2018.
- Zender, C. S.: Mineral Dust Entrainment and Deposition (DEAD) model: Description and 1990s dust climatology, J. Geophys. Res., 108, 4416, https://doi.org/10.1029/2002JD002775, 2003.

https://doi.org/10.5194/acp-2019-785
Preprint. Discussion started: 11 September 2019

Atmospheric Chemistry and Physics Discussions

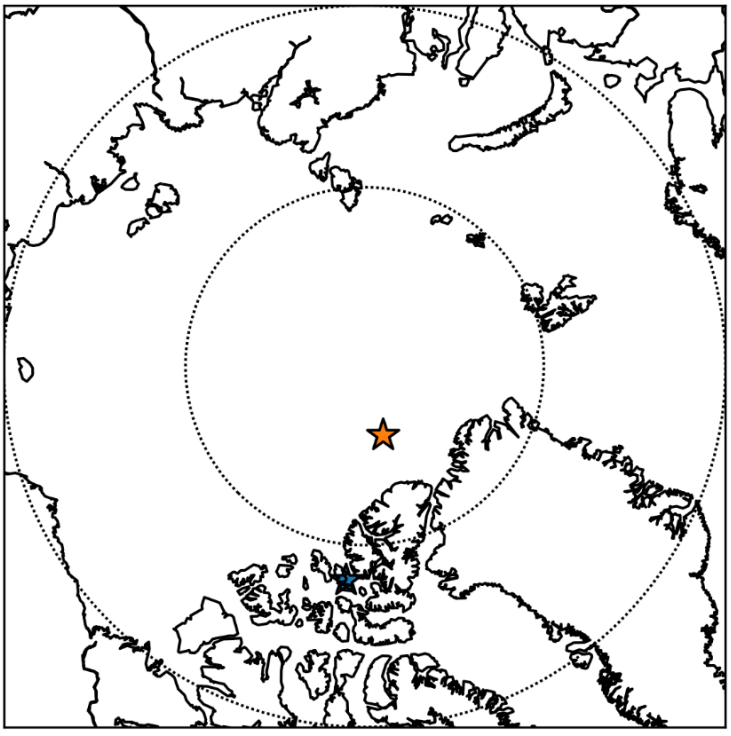

Figure 1. Map of Arctic centred on North Pole. Stars show centre of model grids used in this study: green is Northwest Alert (NW Alert) grid; orange is Axel grid. Grid sizes are approximately 440 km (N-S) x 72 km (E-W).

https://doi.org/10.5194/acp-2019-785
Preprint. Discussion started: 11 September 2019

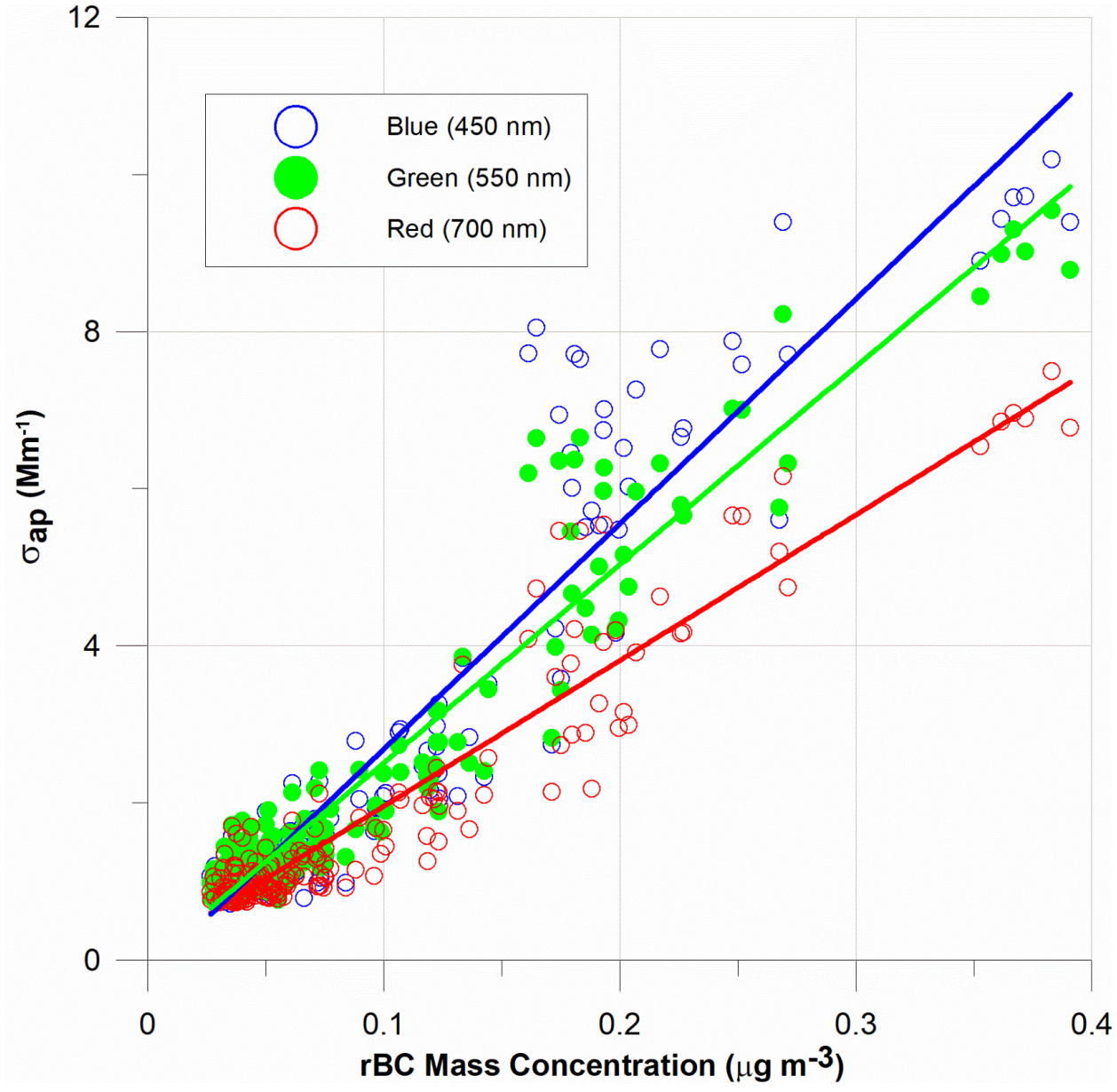

Figure 2. Particle light absorption coefficient (σ_{ap}) at three wavelengths (450 nm, 550 nm and 700 nm) plotted versus refractory black carbon (rBC) mass concentrations for all above-detection-limit data collected during POLAR 6 flights from Alert, Nunavut, Eureka, Nunavut and Inuvik, NWT. Regression lines shown for reference.

https://doi.org/10.5194/acp-2019-785
Preprint. Discussion started: 11 September 2019

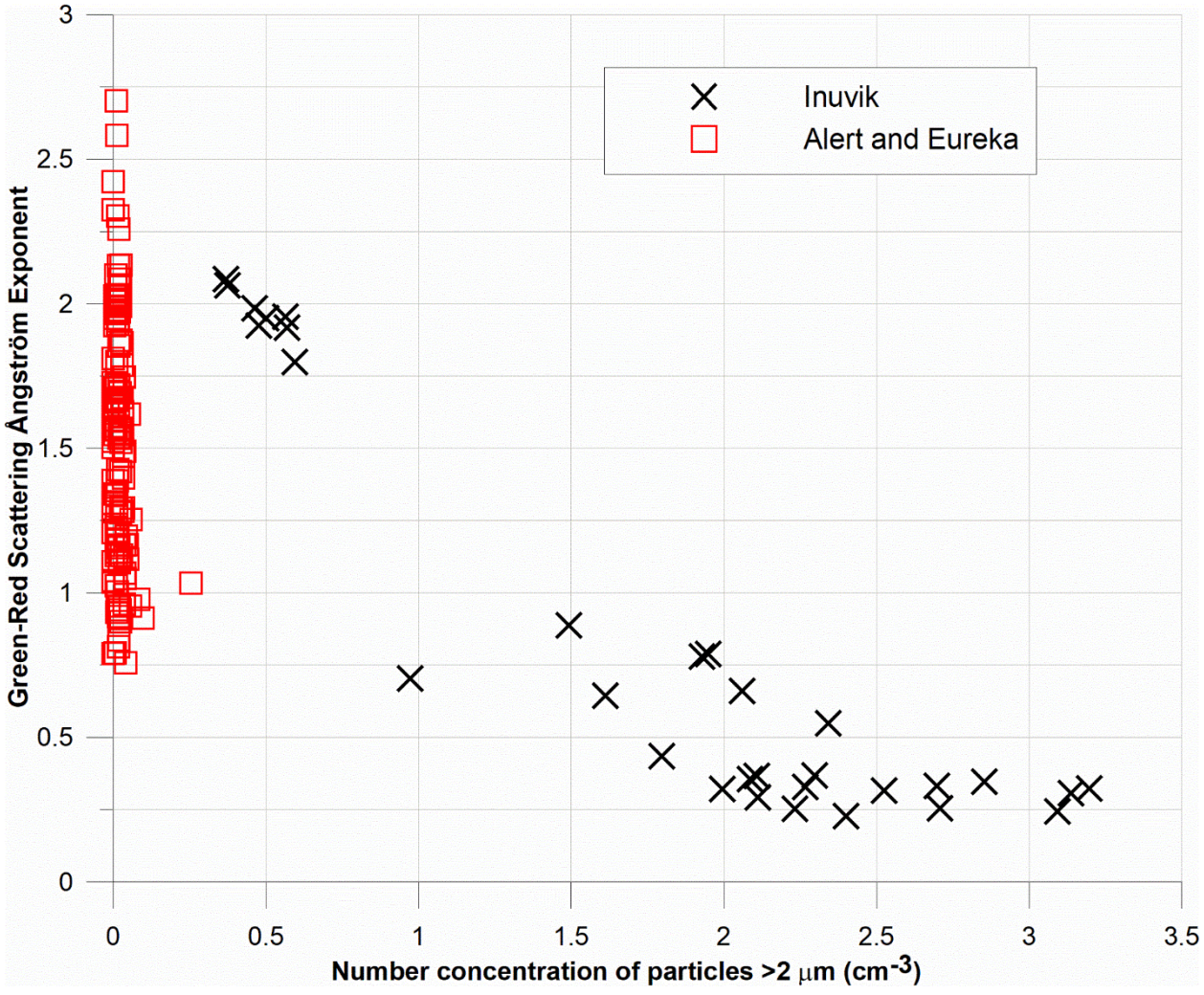

Figure 3. Light-scattering Angstrom exponent between green and red wavelengths plotted versus the number concentrations of coarse particles (<2 μm diameter). Data are separated between those collected during flights from Alert and Eureka (red boxes) and from Inuvik (black crosses).

https://doi.org/10.5194/acp-2019-785
Preprint. Discussion started: 11 September 2019

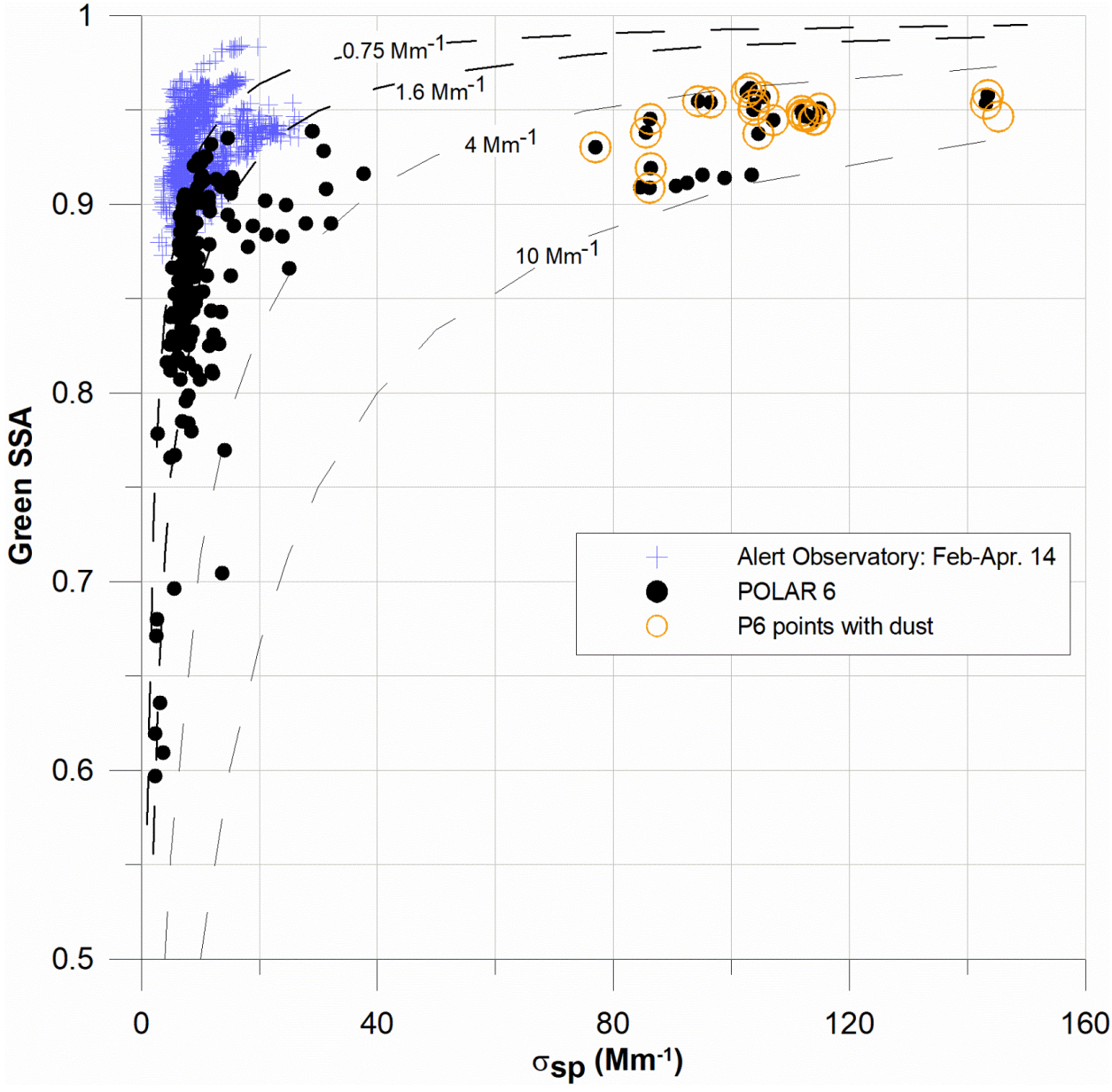

Figure 4. Single scattering albedo (SSA) at the green wavelength (550 nm) plotted versus the particle light scattering coefficient (σ_{sp}) at 550 nm. Data are separated between those collected at the Alert Observatory (blue crosses) and those collected from the POLAR 6 aircraft (black dots). In addition, points influenced most strongly by dust are circled in orange. Line of equal particle light absorption (σ_{ap}) are for reference.

https://doi.org/10.5194/acp-2019-785
Preprint. Discussion started: 11 September 2019

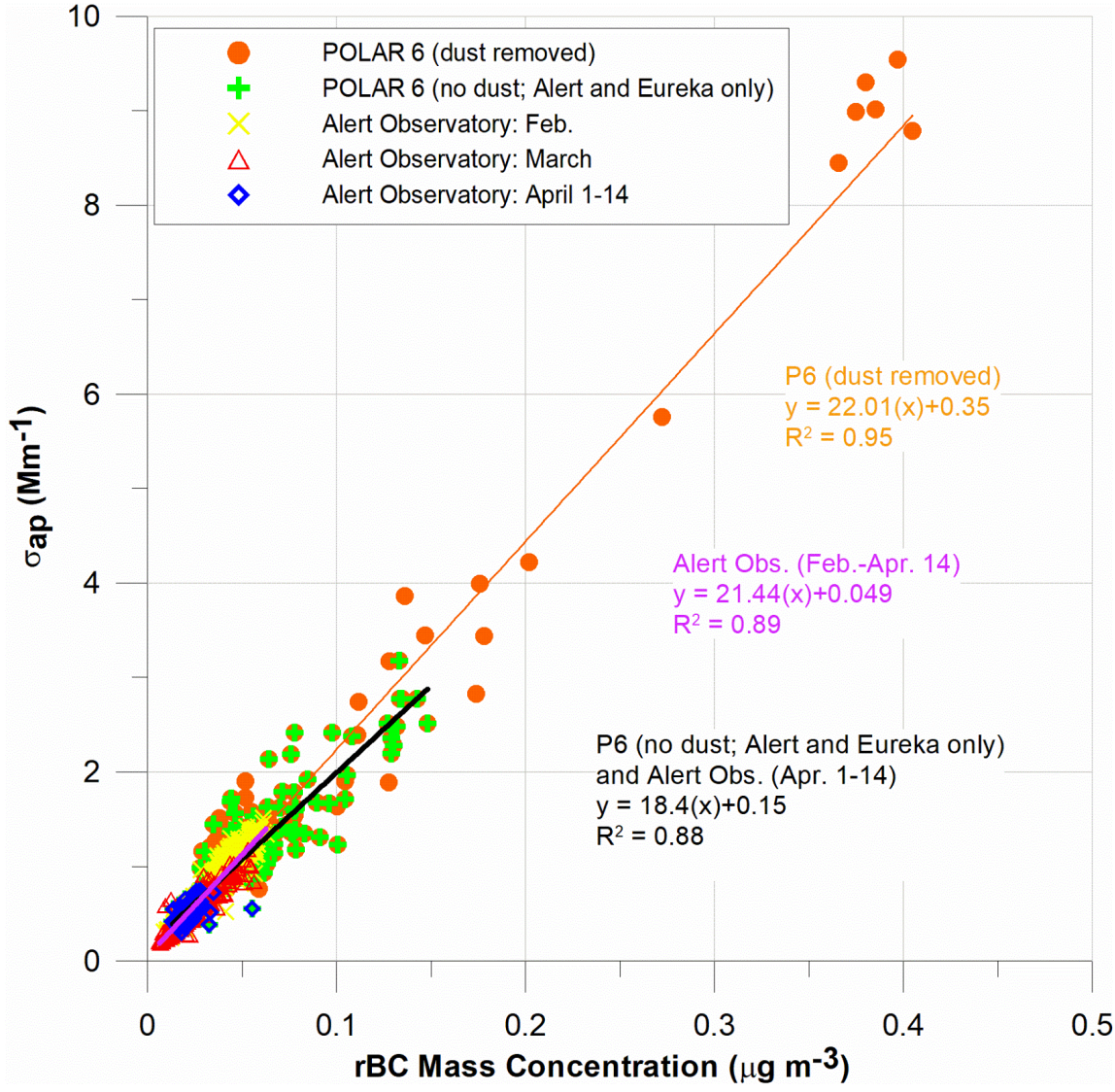

Figure 5. Particle light absorption coefficient (σ_{ap}) at 550 nm plotted versus refractory black carbon (rBC) mass concentrations for all above-detection-limit data collected during POLAR 6 flights from Alert, Eureka and Inuvik, NWT, with major dust influence removed (orange dots), for data collected during POLAR 6 flights from Alert and Eureka only (green crosses) and for data collected at the Alert Observatory. The Alert Observatory data are separated between those collected during February, during March and during April 1-14, where the latter corresponds mostly closely with the POLAR 6 flights out of Alert and Eureka. Regressions are shown for all POLAR 6 data (major dust removed; orange curve), for all Alert Observatory data (purple curve) and for the POLAR 6 data from Alert and Eureka combined with the Alert Observatory data for April 1-14 (black curve).

https://doi.org/10.5194/acp-2019-785
Preprint. Discussion started: 11 September 2019

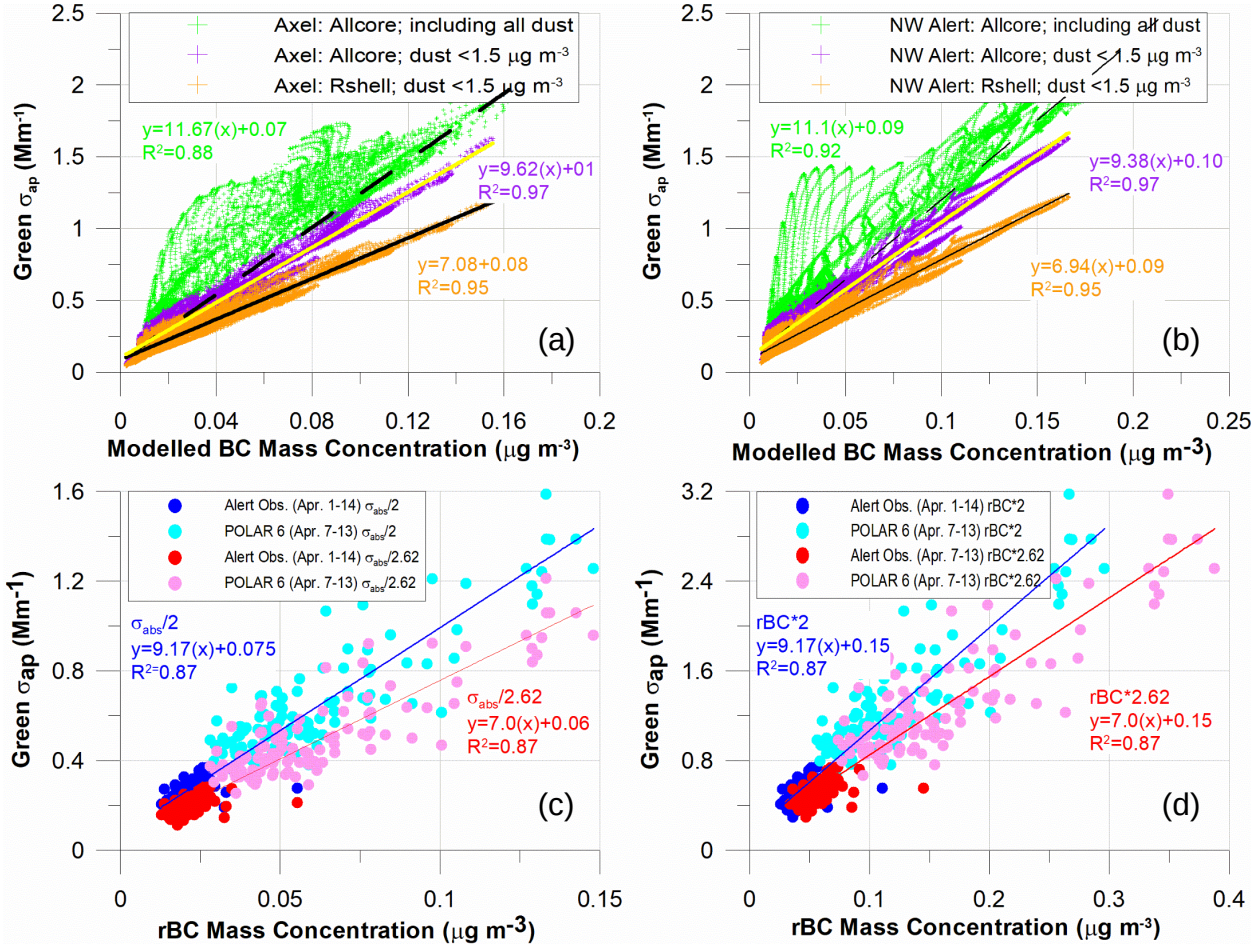

Figure 6. Modelled and observed particle light absorption coefficients (σ_{ap}) at 550 nm plotted versus black carbon and refractory black carbon (rBC) mass concentrations, respectively: a) modelled data for Axel grid showing all data based on the 'Allcore' assumption (green), data based on the 'Allcore' assumption and with dust limited to less than 1.5 μg m^{-3} (purple), data based on the 'Rshell' assumption and with dust limited to less than 1.5 μg m^{-3} (orange); b) as in (a), but for the NW Alert grid; c) POLAR 6 and Alert Observatory (April 1-14 only) data after reduction of the σ_{ap} (division by 2 and by 2.62) to match lower values of the Mass Absorption Coefficient (MAC) for absorption by BC; d) POLAR 6 and Alert Observatory (April 1-14 only) data after increase of BC (multiplication by 2 and by 2.62) to match lower values of MAC for absorption by BC.

https://doi.org/10.5194/acp-2019-785
Preprint. Discussion started: 11 September 2019

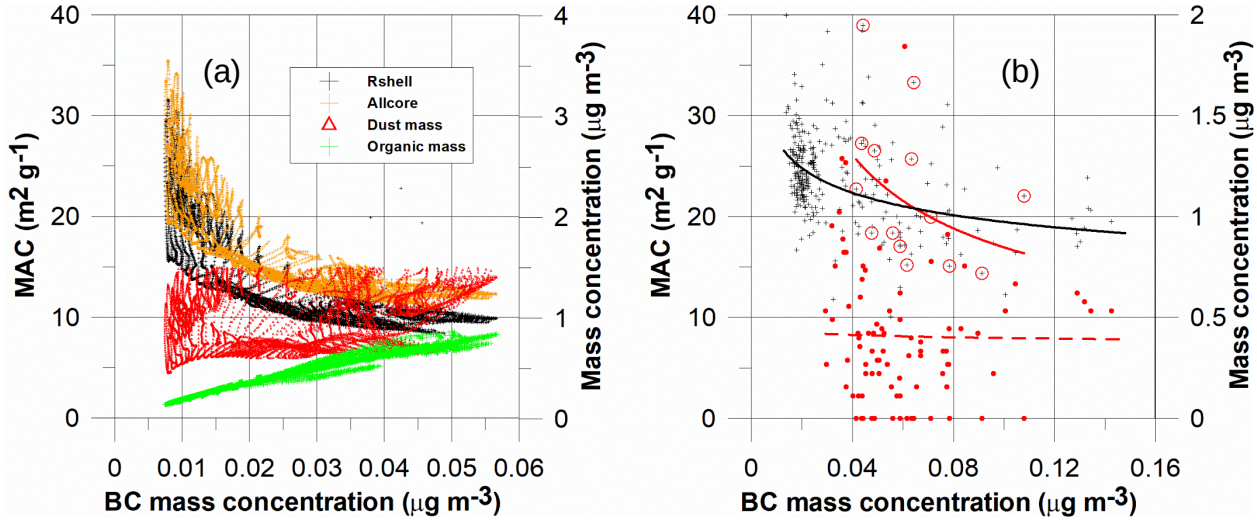

Figure 7. a) Modelled BC Mass Absorption Coefficient (MAC) plotted against modelled BC for the 'Allcore' (black crosses) and the 'Rshell" (orange crosses) assumptions; modelled dust mass concentrations constrained to dust less than 1.5 μg m^{-3} versus modelled BC mass concentrations (red triangles); modelled organic aerosol (OA) mass concentrations versus BC mass concentrations (green crosses); all modelled values are for April 1-14, 2015. b) MAC values from POLAR 6 flights plotted versus measured refractory black carbon (rBC) mass concentrations (black crosses); dust mass concentrations (red dots) estimated from onboard particle size distributions plotted versus rBC mass concentrations; MAC values associated with zero dust points identified (red circles); curve fits to show general tendencies.

https://doi.org/10.5194/acp-2019-785
Preprint. Discussion started: 11 September 2019

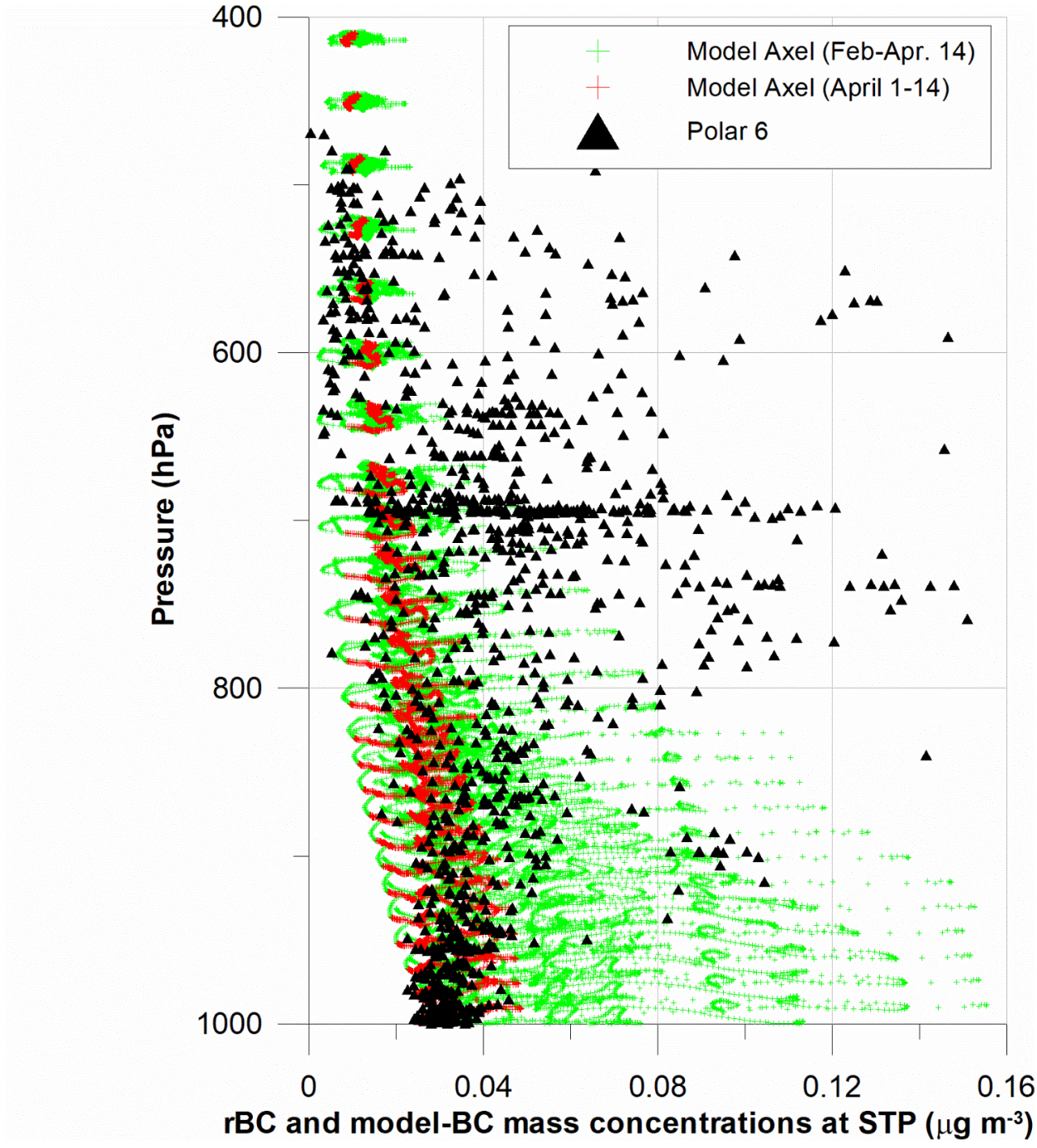

Figure 8. Vertical profile plot of BC mass concentrations from the model for the Axel grid (green crosses for Feb.-Apr. 14, inclusive; red crosses for April 1-14 only) and rBC mass concentrations from the POLAR 6 observations plotted with pressure.

https://doi.org/10.5194/acp-2019-785
Preprint. Discussion started: 11 September 2019

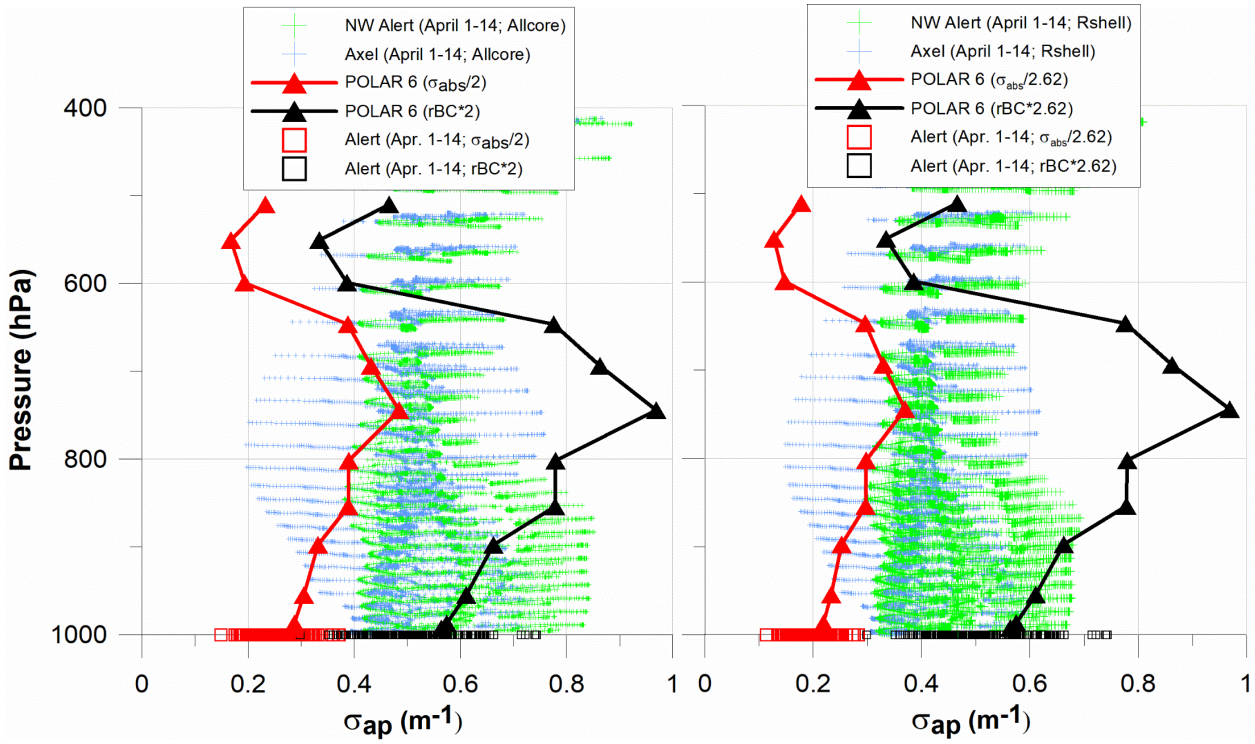

Figure 9. a) Vertical profile plot of σ_{ap} with atmospheric pressure showing median values based on POLAR 6 observations for the absorption overestimation assumption based on $\sigma_{ap}/2$ (red points) and the BC underestimation assumption based on rBC*2 (black points). Data from the Alert Observatory for April 1-14 are shown for the absorption overestimation (red squares) and BC underestimation assumptions (black squares). The corresponding model results for April 1-14 and based on the 'Allcore' assumption are shown by the green crosses for the NW Alert grid and blue crosses for the Axel grid. b) As in a), but the model results are based on the 'Rshell' assumption, and the observation-based points for the absorption overestimation assumption are based on $\sigma_{ap}/2.62$ (red points) and for the BC underestimation assumption are based on rBC*2.62 (black points), which correspond with the modelled MAC value for the 'Rshell' assumption.

https://doi.org/10.5194/acp-2019-785
Preprint. Discussion started: 11 September 2019

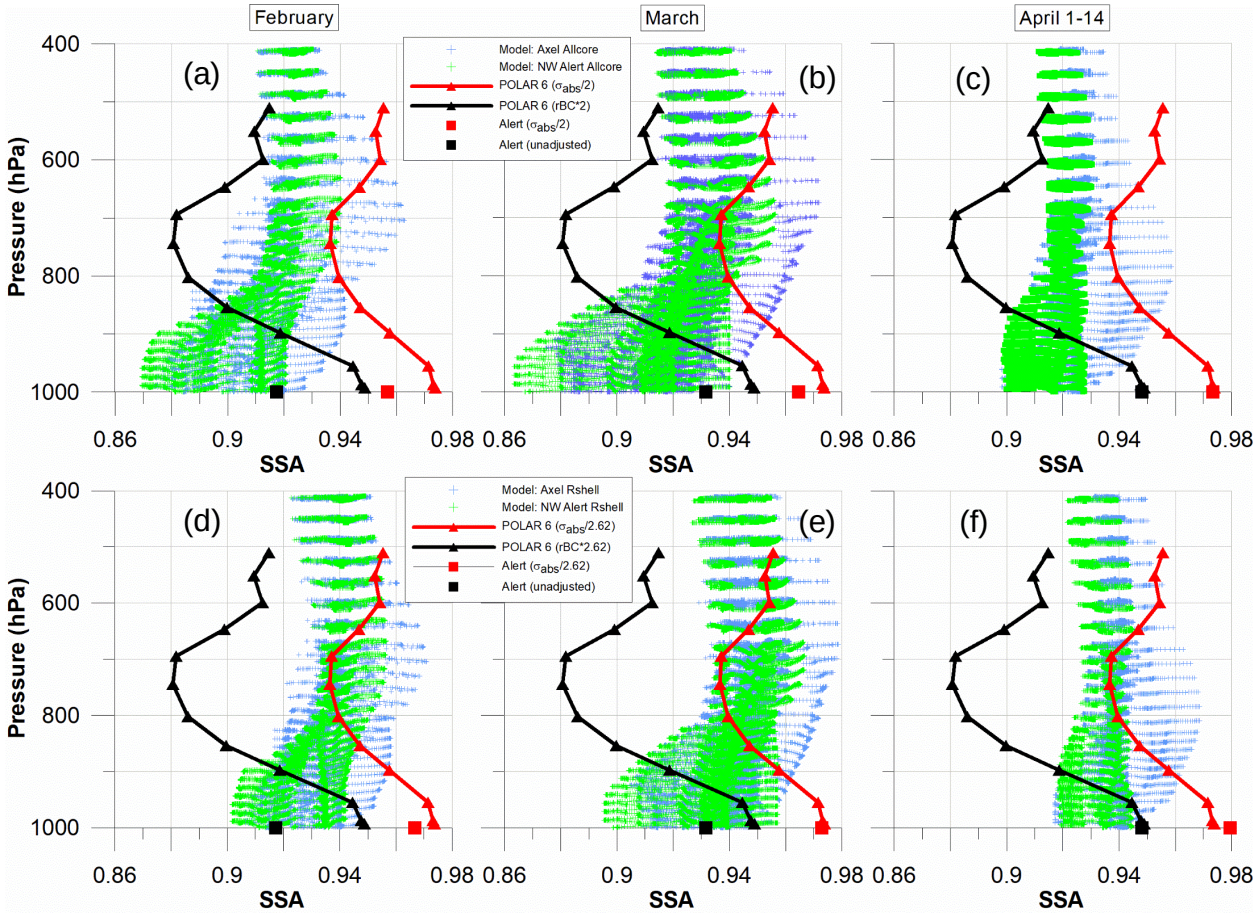

Figure 10. Vertical profile plot of SSA with atmospheric pressure showing modelled results for February (a), March (b) and April 1-14 (c) based on the 'Allcore' assumption and results for February (d), March (e) and April 1-14 (f) based on the 'Rshell' assumption. Median values of SSA from the POLAR 6 observations and the Alert Observatory shown in a, b and c are for the absorption overestimation assumption ($\sigma_{ap}/2$; red points) and the BC underestimation assumption (rBC*2; black points), corresponding to the 'Allcore' assumption. Median values of SSA from the POLAR 6 observations and the Alert Observatory shown in d, e and f are for the absorption overestimation assumption ($\sigma_{ap}/2.62$; red points) and the BC underestimation assumption (rBC*2.62; black points), corresponding to the 'Rshell' assumption.

https://doi.org/10.5194/acp-2019-785
Preprint. Discussion started: 11 September 2019

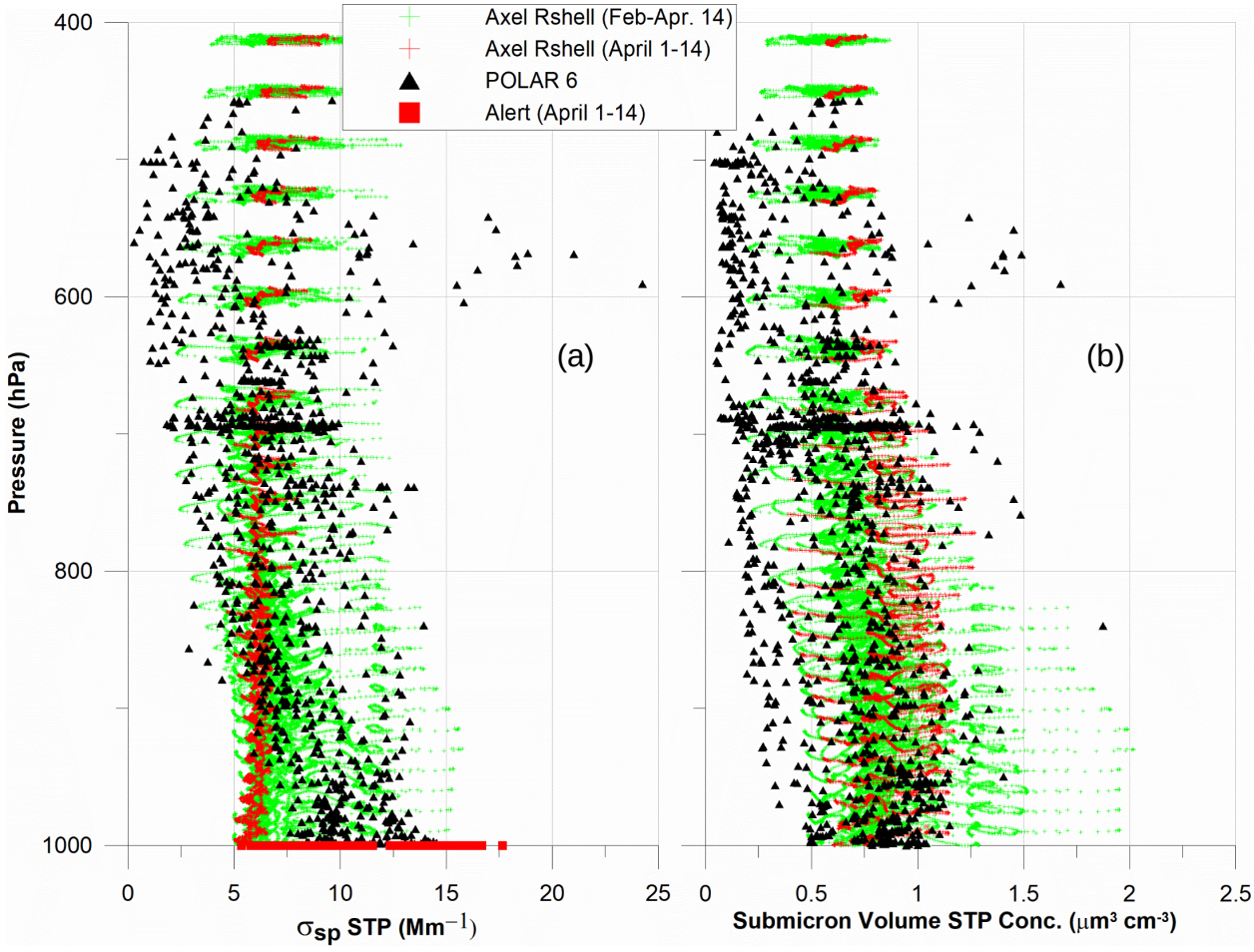

Figure 11. a) Vertical profile plot of σ_{sp} from the model for the Axel grid (green crosses for Feb.-Apr. 14, inclusive; red crosses for April 1-14 only) and σ_{sp} from the POLAR 6 observations plotted with pressure. Also shown are the Alert Observatory σ_{sp} for April 1-14. b) As in a), but for submicron volume concentrations from the model simulations and POLAR 6 observations. Volume concentrations from the Alert Observatory are not shown.

https://doi.org/10.5194/acp-2019-785
Preprint. Discussion started: 11 September 2019

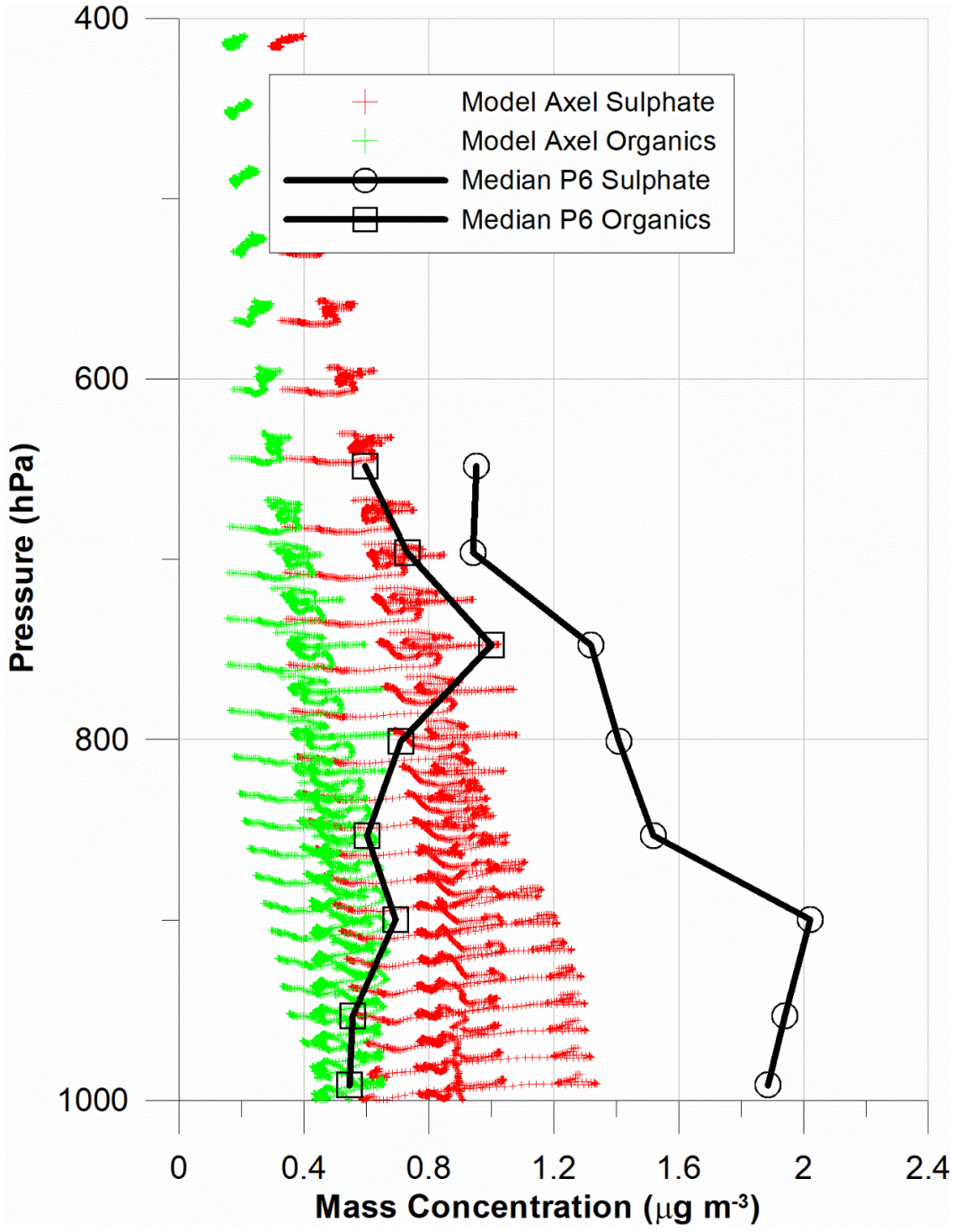

Figure 12. Vertical profile plot of mass concentrations of sulphate and of organics with pressure from the model for the Axel grid for April 1-14 (red crosses are sulphate and green crosses are organics) and median values of the POLAR 6 sulphate (open circles) and organic (open squares) mass concentrations.